SERI/TR-232-2565
DE85016891

November 1985

Engineering Systems Analysis of a Hybrid Quantum/Thermal Process for Fuels and Chemicals Production

D. J. Schell
M. E. Karpuk
SERI

R. E. West
University of Colorado

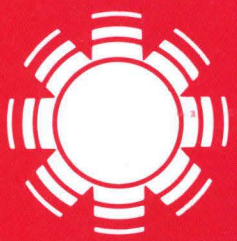

SERI

Solar Energy Research Institute
A Division of Midwest Research Institute

1617 Cole Boulevard
Golden, Colorado 80401-3393

Operated for the
U.S. Department of Energy
under Contract No. DE-AC02-83CH10093

Printed in the United States of America
Available from:
National Technical Information Service
U.S. Department of Commerce
5285 Port Royal Road
Springfield, VA 22161

Price: Microfiche A01
Printed Copy A04

Codes are used for pricing all publications. The code is determined by the number of pages in the publication. Information pertaining to the pricing codes can be found in the current issue of the following publications, which are generally available in most libraries: *Energy Research Abstracts, (ERA); Government Reports Announcements* and Index (*GRA* and I); *Scientific and Technical Abstract Reports (STAR);* and publication, NTIS-PR-360 available from NTIS at the above address.

SERI/TR-232-2565
UC Category: 62c
DE85016891

Engineering Systems Analysis of a Hybrid Quantum/Thermal Process for Fuels and Chemicals Production

D. J. Schell
M. E. Karpuk
SERI

R. E. West
University of Colorado

November 1985

Prepared under Task Nos. 5103.23 and 5101.110
FTP No. 463

Solar Energy Research Institute
A Division of Midwest Research Institute

1617 Cole Boulevard
Golden, Colorado 80401

Prepared for the
U.S. Department of Energy
Contract No. DE-AC02-83CH10093

SERI

PREFACE

The research and development described in this document was conducted within the U.S. Department of Energy's Solar Thermal Technology Program. The goal of this program is to advance the engineering and scientific understanding of solar thermal technology and to establish the technology base from which private industry can develop solar thermal power production options for introduction into the competitive energy market.

Solar thermal technology concentrates the solar flux using tracking mirrors or lenses onto a receiver where the solar energy is absorbed as heat and converted into electricity or incorporated into products as process heat. The two primary solar thermal technologies, central receivers and distributed receivers, employ various point and line-focus optics to concentrate sunlight. Current central receiver systems use fields of heliostats (two-axis tracking mirrors) to focus the sun's radiant energy onto a single, tower-mounted receiver. Point focus concentrators up to 17 meters in diameter track the sun in two axes and use parabolic dish mirrors or Fresnel lenses to focus radiant energy onto a receiver. Troughs and bowls are line-focus tracking reflectors that concentrate sunlight onto receiver tubes along their focal lines. Concentrating collector modules can be used alone or in a multimodule system. The concentrated radiant energy absorbed by the solar thermal receiver is transported to the conversion process by a circulating working fluid. Receiver temperatures range from 100°C in low-temperature troughs to over 1500°C in dish and central receiver systems.

The Solar Thermal Technology Program is directing efforts to advance and improve each system concept through solar thermal materials, components, and subsystems research and development and by testing and evaluation. These efforts are carried out with the technical direction of DOE and its network of field laboratories that works with private industry. Together they have established a comprehensive, goal-directed program to improve performance and provide technically proven options for eventual incorporation into the nation's energy supply.

To successfully contribute to an adequate energy supply at reasonable cost, solar thermal energy must be economically competitive with a variety of other energy sources. The Solar Thermal Program has developed components and system-level performance targets as quantitative program goals. These targets are used in planning research and development activities, measuring progress, assessing alternative technology options, and developing optimal components. These targets will be pursued vigorously to ensure a successful program.

On January 10 and 11, 1983, a workshop hosted by SERI and co-chaired by Dr. Frank Kreith and Dr. Arthur Nozik was held to discuss the possibilities and implications of combining quantum and thermal conversion processes into a hybrid system. As a result of this workshop, SERI initiated work to determine the merits of a hybrid quantum/thermal conversion system. As a part of that effort, this report presents an engineering analysis from a systems perspective evaluating the relative merits of a hybrid system for producing hydrogen.

The authors wish to thank and acknowledge V. K. Mathur of the University of New Hampshire for suggesting caprolactam production with a hybrid solar energy

system. We also wish to thank Tomasz Jansson of National Technical Systems for his help and suggestions, as well as Gordon Gross, Marty Murphy, Mike Connolly, Bruce Parkinson, John Benner, Lee Cole, and Ken Zweibel, all of SERI. We also thank Alan Haught of the United Technology Research Center, John Biddle of the California State Polytechnic University, and David Johnson, Gerald Nix, and Bim Gupta of SERI for their reviews of this report.

Approved for

SOLAR ENERGY RESEARCH INSTITUTE

David H. Johnson

David Johnson, Manager
Thermal Sciences Research Branch

L. J. Shannon

L. J. Shannon, Director
Solar Heat Research Division

SUMMARY

Objective

This study addresses the engineering and cost aspects of a hybrid quantum/thermal conversion system for the production of fuels and chemicals. A cost-sensitivity analysis is done to determine the conditions under which fuels and chemicals production will be economical.

Discussion

Coupling a quantum process (e.g., photochemical, photovoltaic, etc.) to a thermal process is one method of converting solar energy to useful work. A hybrid quantum/thermal system analyzed in this report is illustrated in Figure S-1. This system uses a beam splitter to separate the short-wavelength radiation, which is collected by the quantum receiver, from the long-wavelength radiation, which is collected by the thermal receiver. At the same thermal receiver temperature, a higher efficiency is achieved by the combined system than from either the quantum or the thermal system alone. This will produce a cheaper product if the additional cost of adding another receiver is not too great. However, the highest conversion efficiencies are achieved by a thermal-only system, although at higher receiver temperatures.

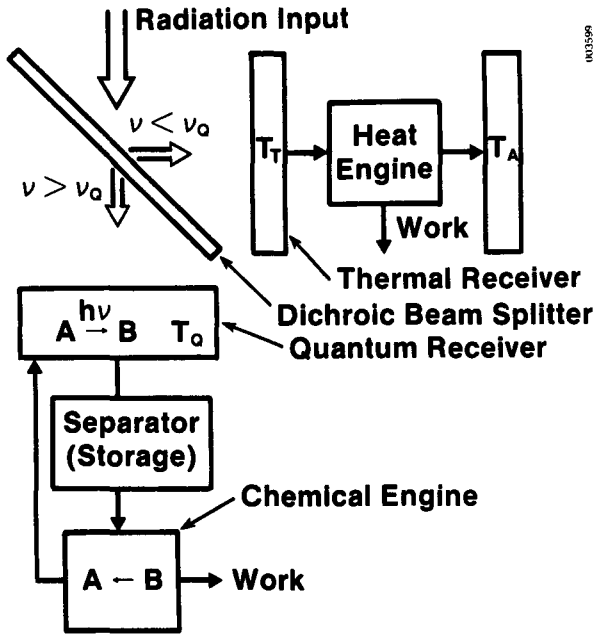

Figure S-1. Thermally Decoupled Combined Quantum/Thermal Conversion.

Since beam splitting is a key aspect of the hybrid system, this report analyzes various methods of beam splitting:

- Selective absorption by a quantum process of short-wavelength radiation, leaving the long-wavelength radiation for the thermal process.
- Dichroic mirrors, which selectively transmit or reflect a portion of the solar spectrum.
- Holograms, which can be made to selectively reflect or transmit a portion of the solar spectrum.
- A fluorescent planar concentrator, which is a dye-impregnated substrate that absorbs short-wavelength radiation and emits fluoresced radiation out of the side of the substrate.

The analysis has shown that holograms and dichroic mirrors are the most effective beam-splitting devices.

Since holograms are effective devices for beam splitting, one design chosen for a collector consisted of a holographic reflector mounted on a heliostat. The use of a heliostat is consistent with the choice of a central receiver power tower for the hybrid plant. The hologram is manufactured to reflect long-wavelength radiation to a thermal receiver on top of the tower and reflect short-wavelength radiation to the quantum receiver, which is placed below the thermal receiver. It is necessary to increase the tower size to support the two receivers.

An analysis that compares a base-case, thermal-only system to the hybrid system was performed to determine the relative cost of the two systems. Hydrogen production was chosen as the common product and the two systems were compared on the basis of the same hydrogen production rate. The base-case system uses a Rankine cycle power plant to convert thermal energy to electrical energy and to then produce hydrogen from an electrolysis process. The hybrid system incorporates the same thermal conversion system, adding a photoelectrochemical process as the quantum system.

The quantum receiver is designed to produce hydrogen and oxygen at separate electrodes using a photoelectrochemical process. Briefly, a semiconductor absorber having the required band gap energy is used to generate electron-hole pairs. Upon recombination at the illuminated cathode surface (semiconductor surface) in contact with an acidic solution, hydrogen is evolved. Concurrently, at the anode surface, oxygen is evolved. A conceptual design employs concentric cylinders for the cathode and anode; the anode is placed inside the hollow cathode, and the entire assembly is encased in a glass tube. Acid solution flows through the tube to remove gases as produced. The glass tube assemblies are mounted vertically around the central tower forming the receiver.

An estimate of the required capital investments and hydrogen production cost is given in Table S-1 for the base-case plant and for three design bases for the hybrid plant. The optimistic case assumes the performance of the photoelectrochemical process at theoretical levels; the pessimistic case assumes performance criteria better than the present state of the art, but they are

values that could be obtained with further research. The results show that a small reduction (13%) in hydrogen production cost is achieved in the optimistic case, compared with the base case plant; production costs are greater in the pessimistic case.

Also included is an analysis of a hybrid system for the production of caprolactam, a high-value chemical. A step in the production of caprolactam can be accomplished photochemically with light in the 365- to 540-nm range. The process is suited to a hybrid conversion scheme, because various processing steps require the input of thermal energy. A hybrid plant requiring only the raw materials would produce caprolactam photochemically with short-wavelength photons, using the remaining solar energy for power and processing needs. The production cost of the hybrid plant is $126/metric ton of caprolactam (excluding raw materials). This compares with $250/metric ton for electricity when mercury lamps are used to generate the photons. Considering that raw materials are half the cost of making caprolactam, a hybrid plant could significantly reduce the price of caprolactam from the current $1,874 per metric ton selling price.

Table S-1. Investment Estimates and Cost of Hydrogen Production (millions of 1980 dollars)

Item	Base-Case Plant	Hybrid Plant Design Basis		
		Optimistic	Moderate	Pessimistic
Heliostat field	121	111	118	126
Central receiver equipment:				
Thermal receiver	12	7	8	9
Photoelectrochemical receiver	--	8	11	18
Tower	12	18	21	32
Photoelectrochemical cooler	--	4	4	4
Transport	12	7	8	9
Storage	12	7	8	9
Power plant	31	17	21	24
Electrolysis plant	25	16	17	19
Balance-of-plant	25	21	24	28
Indirects	62	54	60	70
Total capital investment	312	270	300	348
Hydrogen production cost ($/GJ)	30	26	29	33

Conclusions and Recommendations

This report concludes that

- There is little economic incentive to pursue the development of a hydrogen-producing hybrid plant.

- There is an economic incentive to pursue the development of a hybrid plant to produce caprolactam.
- Further development of beam splitters (holograms, in particular) will be needed to realize the potential of thermally decoupled hybrid conversion.

From these considerations, this report recommends that

- Hybrid systems for hydrogen production not be given any further consideration.
- The feasibility of hybrid conversion for the production of high-value chemicals be investigated (e.g., caprolactam).
- A program be initiated to define the capabilities and limitations of beam splitters, particularly the use of holograms as beam splitters and concentrators.
- Other thermally coupled and decoupled hybrid conversion schemes be investigated, so that the full potential of hybrid conversion systems can be assessed.

TABLE OF CONTENTS

LIST OF FIGURES

LIST OF FIGURES (Concluded)

LIST OF TABLES

SECTION 1.0

INTRODUCTION

The conversion of radiant energy to useful work can be accomplished using either thermal conversion methods such as steam generators, gas turbines, and thermoelectrics, or quantum conversion methods employing photovoltaics and photochemistry, for example. The fundamental limits of the conversion efficiencies of these methods are determined by thermodynamics. The maximum efficiency of thermal processes is given by the Carnot limit. The maximum efficiency of quantum conversion methods has been analyzed by many authors: Shockley and Queisser (1961) for example, for photovoltaics and Ross (1967) and Ross and Hsiao (1977) for photochemical processes. Bolton et al. (1981) have also shown that the thermodynamic, quantum, and photochemical analysis of efficiency limits are all equivalent. A general analysis of conversion efficiency applicable to any conversion process has been developed by Haught (1984) and is the method used in this study.

Haught has presented the idea of a coupled quantum-thermal conversion system in which the energy not used by a quantum conversion process is used as an input to a thermal cycle at the quantum receiver temperature (1984), as shown in Figure 1-1. The quantum η_Q, thermal η_T, and combined η_{Q-T} efficiency of this system are shown in Figure 1-2. Efficiency has been plotted as a function of the receiver temperature T_Q at the optimum cutoff frequency.

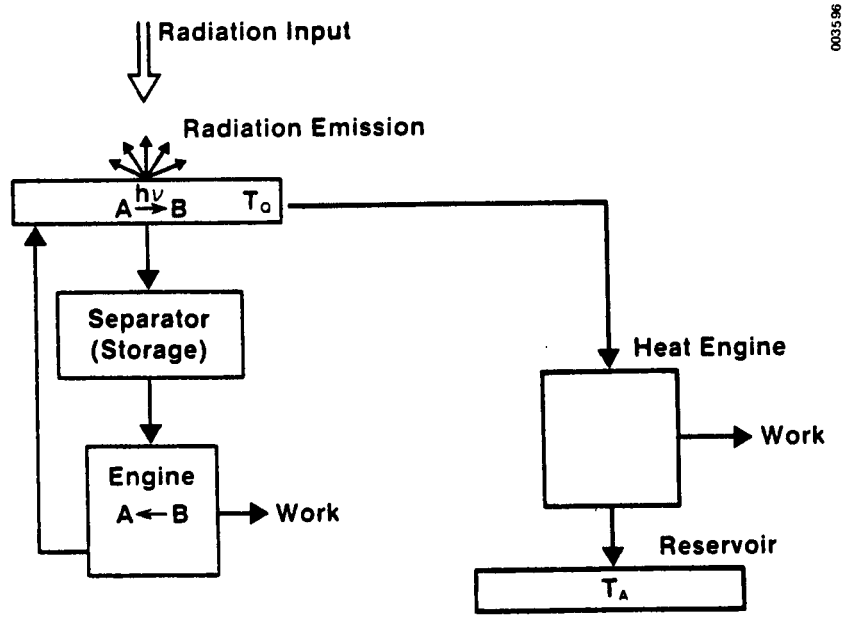

Figure 1-1. Thermally Coupled Combined Quantum/Thermal Conversion

Johnson (1983) extended this analysis to a decoupled quantum/thermal conversion system, as shown in Figure 1-3. In this case, the quantum process is allowed to operate at ambient temperature independent of the thermal receiver temperature. This is accomplished by splitting the solar spectrum at a particular wavelength and sending only photons with energy greater than the required band-gap energy to the quantum receiver. In practice, the quantum receiver is cooled to remove thermalized energy, which represents the difference between photon energy and the Gibbs energy. The quantum, thermal, and combined $\eta_{Q/T}$ efficiency of this system is shown in Figure 1-4, again as a function of the thermal receiver temperature T_T at the optimum cutoff frequency.

Note that at the same receiver temperature, a higher combined efficiency is achieved by the coupled systems, compared with either the quantum or thermal system alone. It is possible to get the same efficiency with a thermal-only system, but a higher receiver temperature is required. Since cost increases with increasing temperature, it should be possible to achieve lower production cost with a thermally decoupled system if the cost of adding a quantum system is not too high. Also, a comparison of Figures 1-2 and 1-4 clearly indicates that at the same temperature, the quantum part of the decoupled system makes a greater contribution to the combined efficiency than the quantum part of the coupled system. This occurs because the quantum receiver is operating at ambient temperature.

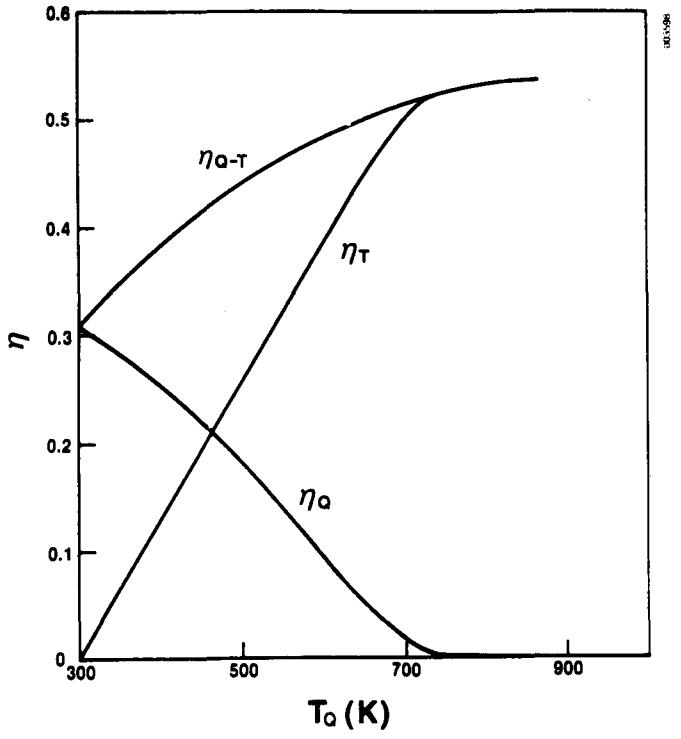

Figure 1-2. Quantum, Thermal, and Combined Efficiency of a Thermally Coupled System for Optimum Cutoff Frequency. Source: Physics Considerations of Solar Energy Conversion, by Alan Haught, United Technologies.

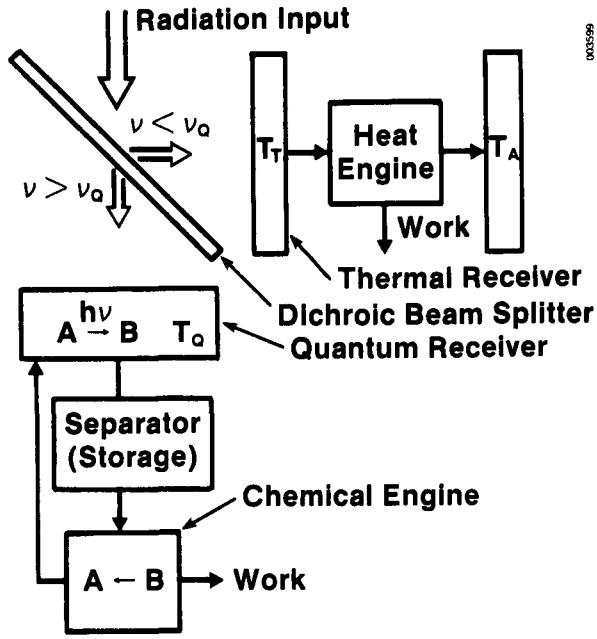

Figure 1-3. Thermally Decoupled Combined Quantum/Thermal Conversion

The idea of combining a photochemical process with a thermal process was explored at a workshop hosted by SERI (Johnson and Karpuk 1983). Some of the major conclusions of the workshop, which guided the development of this work, are as follows:

- Although thermodynamics is a useful tool to help establish the direction of future research, system cost is still the critical element.
- Little is known about the effects of concentrated sunlight on photochemical and photoelectrochemical systems; therefore, these should be investigated.
- The photochemical processes for a hybrid system in which the photochemical reaction is a significant part of the overall process are the ones most likely to be successful.
- The primary emphasis in photoelectrochemistry research has been on liquid-phase systems; however, gas-phase systems or other possibilities may combine better with thermal conversion in a hybrid system.
- Concentrating sunlight has the practical advantage of reducing the receiver size needed, which may make the use of exotic reactors and catalysts more economically attractive.

The intent of this work is to perform an engineering systems study of a hybrid quantum/thermal conversion system for fuel and chemical production. A hybrid system was chosen because the quantum part of the system makes a larger contribution to the overall efficiency. It was therefore necessary to choose a base-case thermal system to compare with the hybrid system. Various collector and thermal plant concepts were reviewed. A central receiver concept was

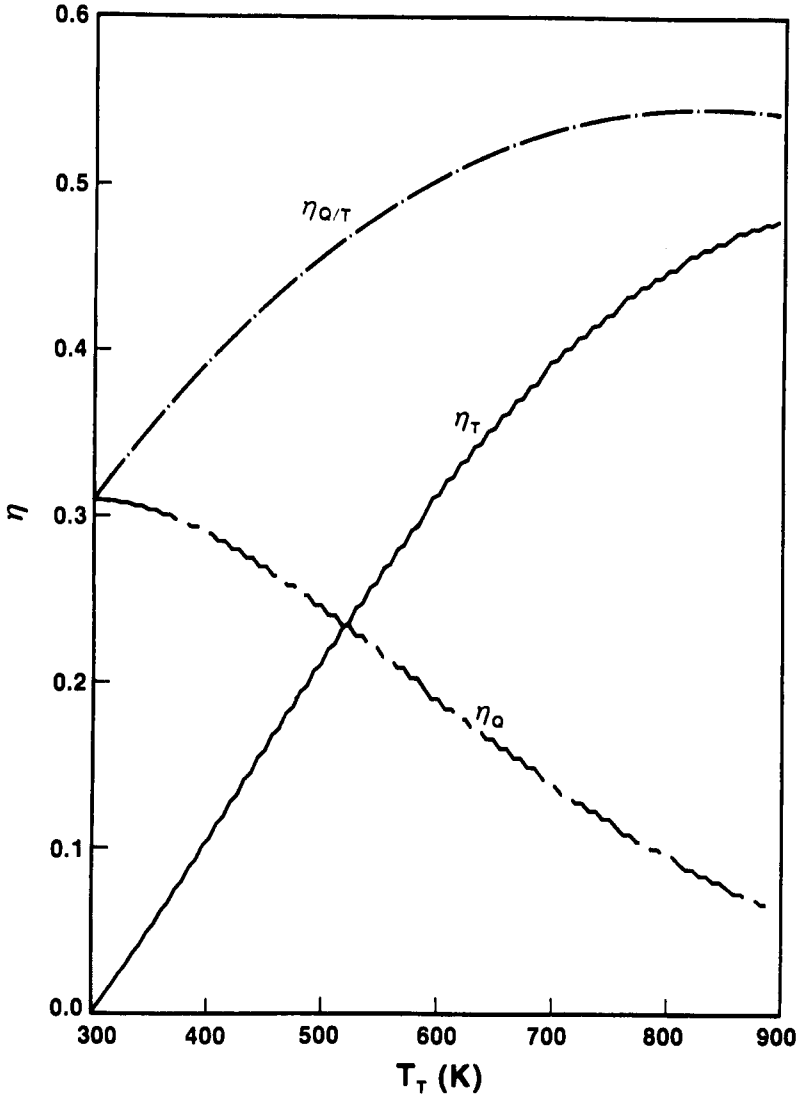

Figure 1-4. Quantum, Thermal, and Combined Efficiency of a Thermally Decoupled System for Optimum Cutoff Frequency

chosen because a centralized fuel production facility appears to be more attractive economically than a decentralized facility (e.g., one using flat-plate collectors). A decentralized facility would require raw material transport to, and product collection from, each collector. Moreover, central receivers can achieve the high temperatures and concentrations needed to realize significant cost reductions.

The product for the quantum system was chosen after several thermochemical and photochemical fuels and chemicals production processes were reviewed. Hydrogen was chosen as the product because of its potential as a fuel and as a

synfuel feedstock, and because of the variety of research and development work that has already been done on hydrogen production methods. With the product and plant type chosen, the base-case, thermal-only system is configured to generate electricity from a Rankine-cycle heat engine to run an electrolyzer that generates hydrogen and oxygen. The hybrid plant is configured to generate hydrogen from the thermal part of the plant using the base-case thermal process; a photoelectrochemical process breaks down water into hydrogen and oxygen for the quantum system. The two plants are analyzed for efficiency and cost based on the same production rate, and the resulting numbers for hydrogen production cost are compared.

In Section 2.0 of this report, the various methods of splitting the solar spectrum at a particular wavelength are reviewed and analyzed. The methods with the greatest efficiencies are then analyzed further for use with a central receiver/heliostat plant. In Section 3.0, the base-case thermal plant and hybrid plant are presented and discussed. A process for caprolactam (a chemical used to manufacture nylon-6) production using a photochemical process is also analyzed. This process was reviewed briefly because it is a chemical production method uniquely suited to a hybrid plant, since a large percentage of the solar spectrum is used by the photochemical process and thermal energy is needed for several processing steps. Our conclusions and recommendations are presented in Section 4.0.

SECTION 2.0

SOLAR BEAM-SPLITTING ANALYSIS

The key feature of a hybrid quantum/thermal conversion system is the splitting of solar radiation into long- and short-wavelength components. The short wavelengths are used by a quantum process and the long wavelengths are used in a thermal process. This important step thermally decouples the quantum from the thermal process.

The purpose of this section is to identify and analyze methods of beam splitting. How can the solar spectrum be split at a chosen wavelength and each part sent to a separate receiver? Can the separated beams be concentrated, and how effectively can the splitting be achieved? To answer these questions, methods of beam splitting were identified that have the potential to work in a hybrid quantum/thermal conversion system. After the methods were identified, models were developed and quantitative performance estimates were made.

2.1 BEAM-SPLITTING PROCESSES

Several promising beam-splitting methods were selected for analysis for their potential as beam splitters and adaptability to a hybrid quantum/thermal process. These methods are selective absorption, dichroic mirrors, holographic concentrators, and fluorescent planar concentrators. Selective absorption refers to direct absorption of short-wavelenth radiation by a quantum process, leaving the unabsorbed portion for the thermal process. Dichroic mirrors are thin layers of semiconductive or dielectric material coated onto a glass substrate, selectively transmitting and reflecting portions of the solar spectrum. Holographic concentrators are thin holograms that diffract a portion of the spectrum and can reflect the beam in the same manner as a dichroic mirror or focus the beam much like a concentrator. Fluorescent planar concentrators consist of a dye-impregnated substrate that absorbs over a particular wavelength band and reradiates out of the side of the collector at a slightly lower frequency.

The following sections present a more detailed discussion of each method, showing the model developed and the results obtained.

2.1.1 Methodology

The objective of this study was to quantify the beam-splitting performance of each of the methods. Efficiency is used to refer to the fraction of energy available to either the quantum or thermal process. This fraction depends on the wavelength at which the beam splitter is to separate. The shorter the wavelength, the smaller the fraction of the energy that is potentially available to the quantum process; conversely, a greater fraction is then available to the thermal process.

This observation points out a significant feature of beam splitters for use in a hybrid conversion system: a method that may not be particularly good at

splitting and separating the short wavelengths from the long wavelengths may not necessarily penalize the system, since, depending on process configuration, this energy could be used by a thermal process. The optical losses associated with splitting the beam are a more overriding concern than is obtaining good separation. The total losses over the entire spectrum divided by the total energy available in the solar spectrum is also shown in the results to be presented. The energy loss plus the energy diverted to the quantum process and the energy diverted to the thermal process equal the input energy. These numbers indicate only the efficiency of beam splitting, not the efficiency at which energy will be used by the quantum or thermal process.

The choice of the particular wavelength at which to separate the beam is dictated by the choice for a quantum system, since the band gap of the quantum process specifies the maximum wavelength of radiation that is useful to the quantum process. The maximum utilization of the short-wavelength component is achieved by matching the required band gap to the separation or cutoff wavelength. To keep the analysis general at this point in the study, beam splitting efficiency is analyzed as a function of cutoff wavelength or band gap of an unspecified quantum process. The trends were as expected, with increasing cutoff wavelength; a larger fraction of the energy is available to the quantum process and a smaller fraction is available to the thermal process. Short- and long-wavelength components now refer to all wavelengths shorter or longer than the cutoff wavelength, respectively.

All methods analyzed assumed normal incidence and an AM 1.5 solar spectrum (Matson et al. 1981). To model any of the beam-splitting methods accurately it is necessary to consider losses and assumptions associated with the path to the quantum and thermal receivers separately. The differences between the quantum and thermal paths will be discussed further in the next section. Furthermore, holographic concentrators and fluorescent planar concentrators are relatively new technological developments, still requiring more research and development. Thus, complete certainty was not possible in the results obtained for these methods. Since improvements in the technology are expected, two cases are presented: the current state of the technology and future theoretical performance. The results presented for selective absorption and dichroic mirrors used real performance data.

The analysis of all of these beam-splitting methods relied upon several simplifying assumptions and estimates of performance data when they were not available. As such, there is the possibility of variance from the true performance of these devices, although the numbers are considered accurate enough to make viable performance estimates.

2.1.2 Beam-Splitting Methods

2.1.2.1 Selective Absorption

Perhaps the simplest method of beam splitting is to directly absorb the short wavelengths of interest in a quantum process, leaving the unabsorbed longer wavelengths for use in a thermal process. In this case, the cutoff wavelength is fixed by the band gap of the quantum process. The disadvantage of this

approach is that a large fraction of the longer wavelengths is also lost or absorbed by the system.

Figure 2-1 shows the model used to analyze the selective absorption case. This is based upon the flat-plate collector designed by Biddle and Peterson (1983) for a solar photochemical reactor. It consists of two glass plates (0.3 cm thick) separated by a 1.0-cm-thick water layer, which contains the photo-sensitizer necessary to dissociate water. The 1.0-cm-thick layer is needed to obtain maximum absorption by the photo-sensitizer. Radiation not used by the quantum process is allowed to pass through the reactor and is available for collection by the thermal receiver, minus the losses that occur traversing the reactor.

A 4.0% reflectance loss of incident radiation was assumed to occur at the top air-glass interface, as given by the Fresnel reflection coefficient. For purposes of calculation, the liquid layer was assumed to be water. This makes the reflection coefficient at the glass-water interface small enough (0.5% as calculated from the Fresnel equations) to be ignored. Since the fraction of energy involved in multiple reflections along the interface is also small, it was ignored as well.

Now, considering the path of short-wavelength radiation to the quantum receiver, the first loss occurs in the form of reflection at the top surface. The second loss occurs as absorption by the glass and was determined from the

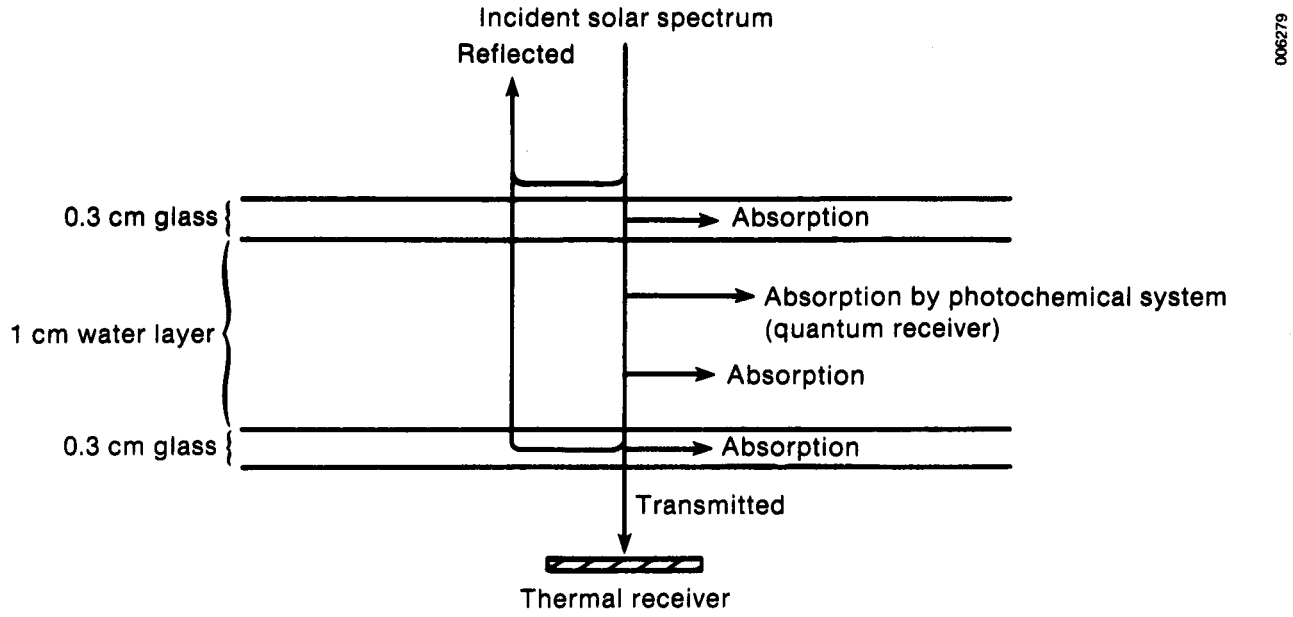

Figure 2-1. Model for a Selective Absorption Reactor

solar transmission characteristic of a low-iron glass. Of the remaining short-wavelength radiation reaching the water layer, 1.0% was assumed to have been absorbed by the water, and the remaining fraction was totally absorbed or useful to the quantum system.

The path of the long-wavelength component is slightly more complicated and involved significantly greater losses. This is due to the longer pathlength which the radiation must traverse and the higher attenuation coefficients for longer wavelength radiation. Again, 4.0% is loss at the top air-glass interface. Absorption by the glass was determined from glass transmittance data and absorption by the water was determined from absorption coefficients (Optical Society of America 1978). Of the remaining energy reaching the bottom air-glass interface, another 4.0% was assumed to have been reflected, and the remaining energy transmitted to the thermal receiver.

All individual losses have been combined into a single loss term for the system. This included the reflected components and absorption by the glass and water of both short- and long-wavelength radiation.

The results of the analysis for selective absorption are shown in Figure 2-2. Note that at the higher cutoff wavelengths, the losses are slightly lower. This is because the radiation used by the quantum process follows a shorter path length, and thus lower overall losses are achieved by diverting a greater fraction to the quantum process. The losses are high (approximately 45%), which indicates that selective absorption may not be the preferred choice for a hybrid system.

2.1.2.2 Dichroic Mirror

Dichroic mirrors consist of thin, semiconductive, metal/dielectric, or dielectric coatings placed onto a glass substrate. Dielectric coatings are common on architectural glass for reducing building air conditioning load by reflecting the visible portion of the spectrum. Semiconductive and metal/dielectric coatings are used on window glass for passive solar applications where visible light is transmitted and infrared is reflected. The wavelength at which the transition between reflecting or transmitting takes place is adjusted by varying the electron doping levels in the conductive coatings. This allows a particular cutoff wavelength to be chosen to match the band gap of the quantum process.

The model used to analyze the performance of dichroic mirrors is shown in Figure 2-3. This model assumes that radiation is reflected above the cutoff wavelength and transmitted below it. Below the cutoff wavelength, the radiation must pass through the 0.3-cm-thick glass substrate with some losses and then be collected by the quantum receiver. Radiation above the cutoff wavelength is reflected and directly collected by the thermal receiver.

The data used to analyze the transmittance of this mirror were estimated from manufacturer-supplied data from 300 nm to the chosen cutoff wavelength for a

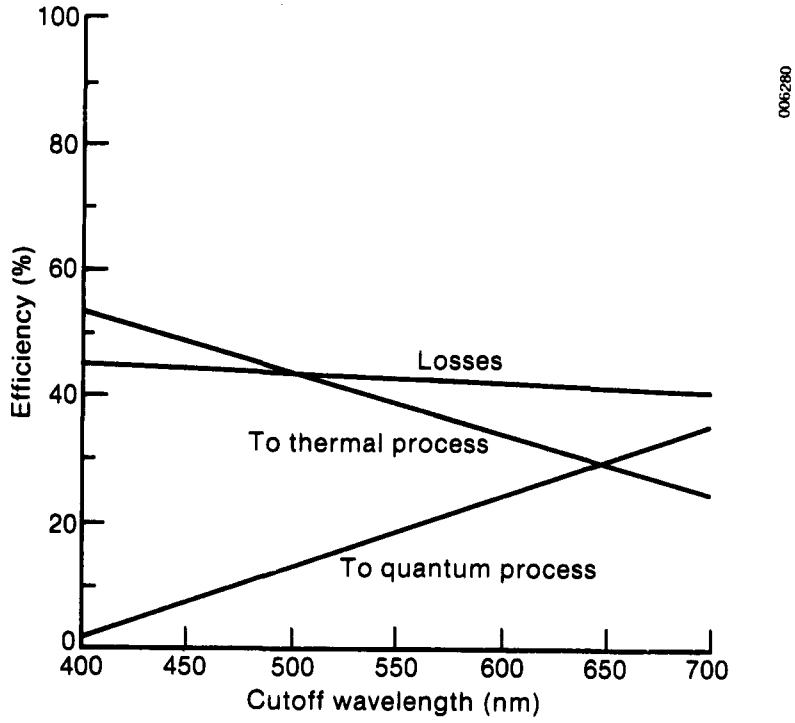

Figure 2-2. Selective Absorption Results

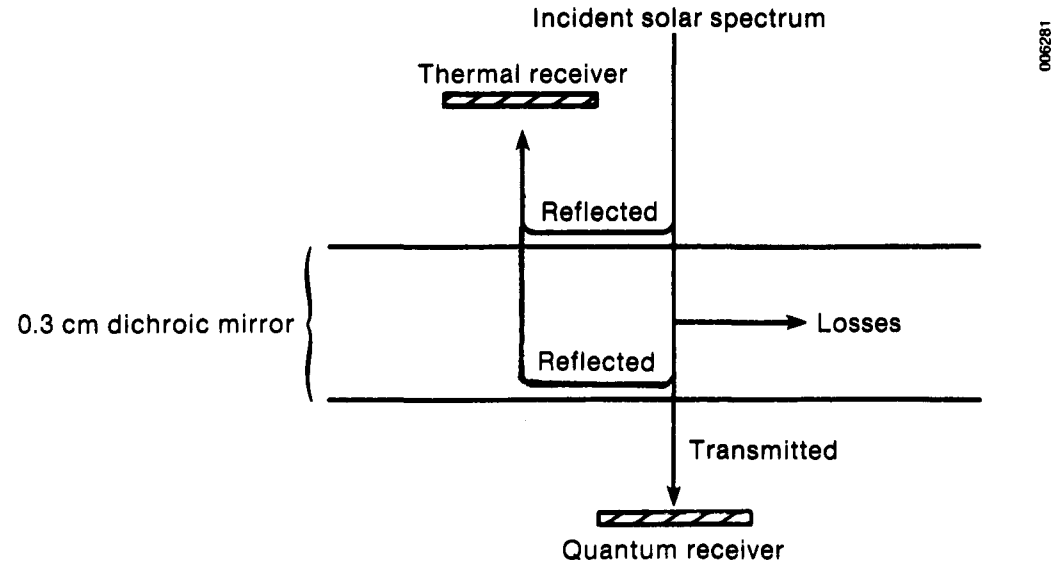

Figure 2-3. Dichroic Mirror Model

short-wave pass filter (Corian Corporation 1983). The effective index of refraction of the coating was 1.7, giving a reflection coefficient of 6.7% from the Fresnel equations.

The short-wavelength component below the cutoff wavelength first loses 6.7% of the incident radiation at the top surface, which is reflected to the thermal receiver. The fraction transmitted through the glass was estimated at 40% for wavelengths below 415 nm and 65% from 415 nm to the chosen cutoff wavelength. The remaining energy below the cutoff wavelength was considered lost. The effect of reflection at the second interface and multiple reflections have been included in the transmittance data.

For the long-wavelength component above the cutoff wavelength, the surface was assumed to reflect 85% of the incident radiation; this is comparable to a good mirror. The other 15% was assumed to have been absorbed by the glass and was considered a loss.

The results of this analysis are shown in Figure 2-4. All loss mechanisms, absorption and scattering, for both short- and long-wavelength radiation have been grouped into the single loss term. The trend is as we expected: with increasing cutoff wavelength, increased energy is available to the quantum process and decreased energy is available to the thermal process. Losses are nearly constant, but do increase slightly with increasing cutoff wavelength; this is because the assumed 15% absorption losses for wavelengths above the cutoff are lower than absorption losses occurring below the cutoff wavelength.

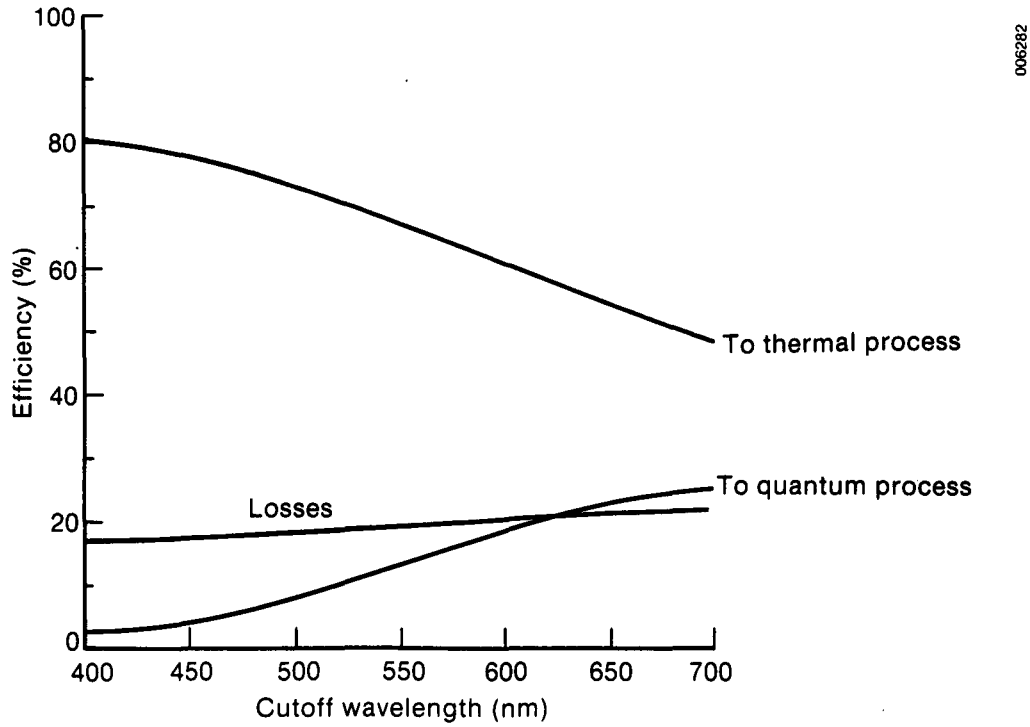

Figure 2-4. Dichroic Mirror Results

Dichroic mirrors are not in themselves concentrating devices, but they can function in much the same manner as a heliostat to obtain concentration, as limited by the present state of solar thermal technology.

2.1.2.3 Holographic Concentrator

Holographic concentrators (HC) are relatively new developments in concentrator technology. To illustrate the basic concept, consider the technique of recording an interference pattern from a reference light beam and an object light beam onto a photographic film. Upon illumination of the recorded pattern on the film, an image of the original object is produced. If the reference beam is sunlight and the object originally illuminated a solar concentrator, then illumination by sunlight produces a focused beam of concentrated light. This offers the possiblity of a lightweight hologram that can concentrate sunlight using diffractive optics. The pattern is easily copied and thus economical to produce.

Ludman has studied broadband HC for focusing and concentrating sunlight (1982). Recent studies by Bloss et al. (1982) and National Technical Systems (1983) have looked at the ability of holograms to split and focus selected wavelength ranges of the solar spectrum. This is accomplished with high-efficiency Bragg holograms. However, high efficiency can only be achieved in a narrow-wavelength range. To achieve a broader range, a series of holograms, or subholograms, are sandwiched together into a single optical element and supported by glass or plastic sheets.

The model used to analyze HC is shown in Figure 2-5. The geometry chosen and data used were from the report by National Technical Systems (1983). This hologram operates by reflecting short-wavelength radiation and allowing longer wavelengths to pass through. The reflected short-wavelength component was estimated from experimental data for a single hologram. Since this represented only a narrow wavelength region, it was assumed that the same performance could be extended from 300 nm to the chosen cutoff wavelength. Above the cutoff wavelength there is no reflected component.

Transmission through the hologram was determined in the same manner as reflection by extending transmission data for a single subhologram from 300 nm to the chosen cutoff wavelength. Subtracting the reflected and transmitted components from the incident radiation left a 25%-35% loss. Since no data were available on transmission of the infrared radiation through these holograms, it was assumed that above the cutoff wavelength, 25% of the incident radiation was loss and the rest transmitted.

The results of this analysis are shown in Figure 2-6 for a hologram analyzed with experimental data. As shown, losses are between 25% and 35% of the total energy available. Not included are losses associated with a cover glazing over the hologram.

The analysis above has only considered the current state of the technology for HC. The theoretical performance of these devices could be much greater; the maximum efficiency is 92%, limited only by Fresnel losses. Thus, the analysis was redone assuming 10.0% losses across the entire spectrum; the extra 2.0%

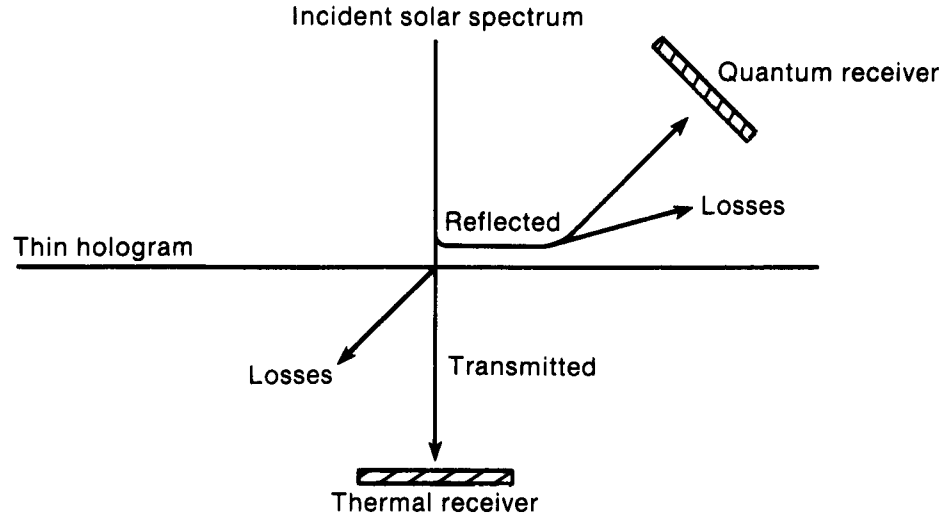

Figure 2-5. Model Used for a Holographic Concentrator

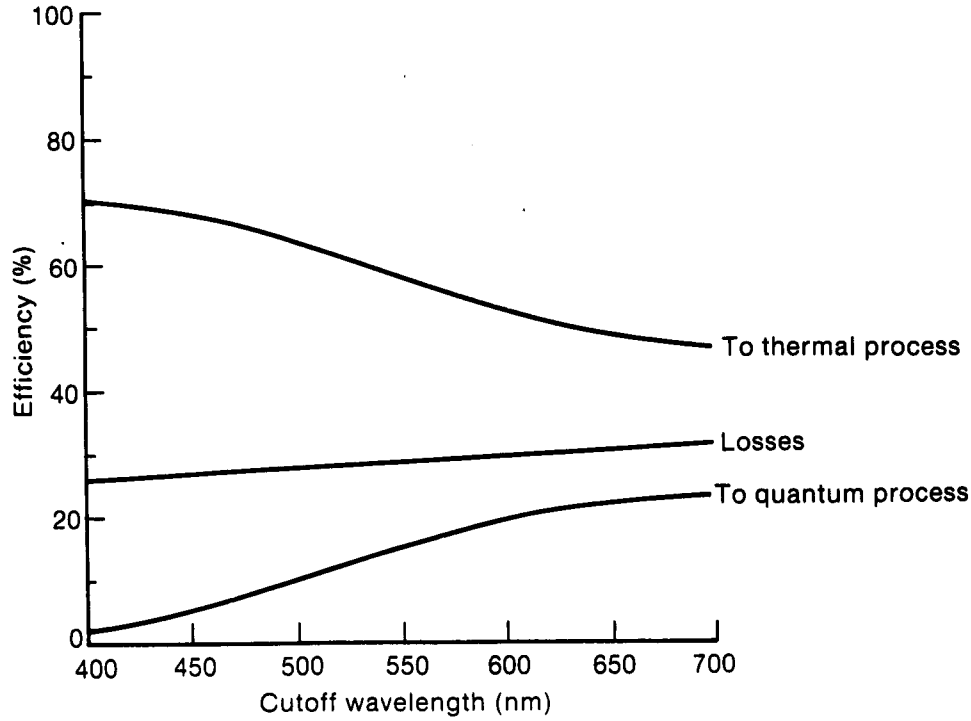

Figure 2-6. Results for an Experimental Holographic Concentrator

was for support media losses. It was also assumed that 90.0% of the solar spectrum below the cutoff wavelength was reflected to the quantum receiver and nothing transmitted, and above the cutoff wavelength, 90.0% of the solar spectrum was transmitted and none reflected.

Using the assumptions above for the theoretical case, the results are shown in Figure 2-7. Note that a larger fraction of the solar energy is now available for both the quantum and thermal processes.

2.1.2.4 Fluorescent Planar Concentrator

A fluorescent-dye-impregnated sheet that collects solar radiation and emits the fluoresced radiation out of the side of the sheet has been reviewed and studied by many people. Goetzberger and Witter (1981), Herman (1982), and Friedman (1980) have all extensively reviewed fluorescent planar concentrators (FPC). Batchelder et al. (1979, 1981) have carried out an extensive experimental study of the performance and efficiencies of FPC. Offenhartz et al. (1983) have evaluated various inorganic dyes for use with FPC. More recent studies by Sansregret et al. (1983) and Thomas et al. (1983) have looked at the losses that limit the efficiency and concentrating ability of these collectors.

FPC devices consist of a transparent flat plate doped with a molecule that efficiently fluoresces when exposed to light in its absorption band. In prior work, the plate or matrix material has been polymethylmethacrylate (PMMA), an inexpensive material easily doped with the dye molecule. The dye molecule absorbs radiation and then fluoresces isotropically at a longer wavelength. The difference in energy between the absorption and the emission band is the Stokes shift energy loss. Only a fraction of the emitted radiation travels the length of the collector, because of successive internal reflections from the upper and lower surfaces of the plate. The fraction of light loss through the surface is governed by the index of refraction of the matrix material, which determines the critical angle θ_c for internal reflection. For PMMA, the index of refraction is 1.49; 74% of the light is emitted at an angle greater than θ_c and is trapped by the collector, as shown in Figure 2-8. The other fraction of light is emitted at an angle less than the critical angle, and thus it defines a cone of light that escapes out of the surfaces of the plate.

Other loss mechanisms that limit the efficiency of the FPC are transport and dye losses. Transport losses include matrix absorption and scattering, dye reabsorption, and internal reflection inefficiencies. Dye losses are incomplete absorption and the quantum efficiency for fluorescence. Incomplete absorption is not an overriding concern for a quantum/thermal conversion system, since the unabsorbed photons are available to the thermal process.

The model used to analyze the FPC is shown in Figure 2-9. Short-wavelength radiation is absorbed by the dye and emitted to the quantum receiver minus losses. The long-wavelength component travels through the matrix to the thermal receiver minus absorption and reflection losses. For this analysis, the collector was assumed to be a 40-cm x 40-cm x 0.3-cm sheet made of PMMA.

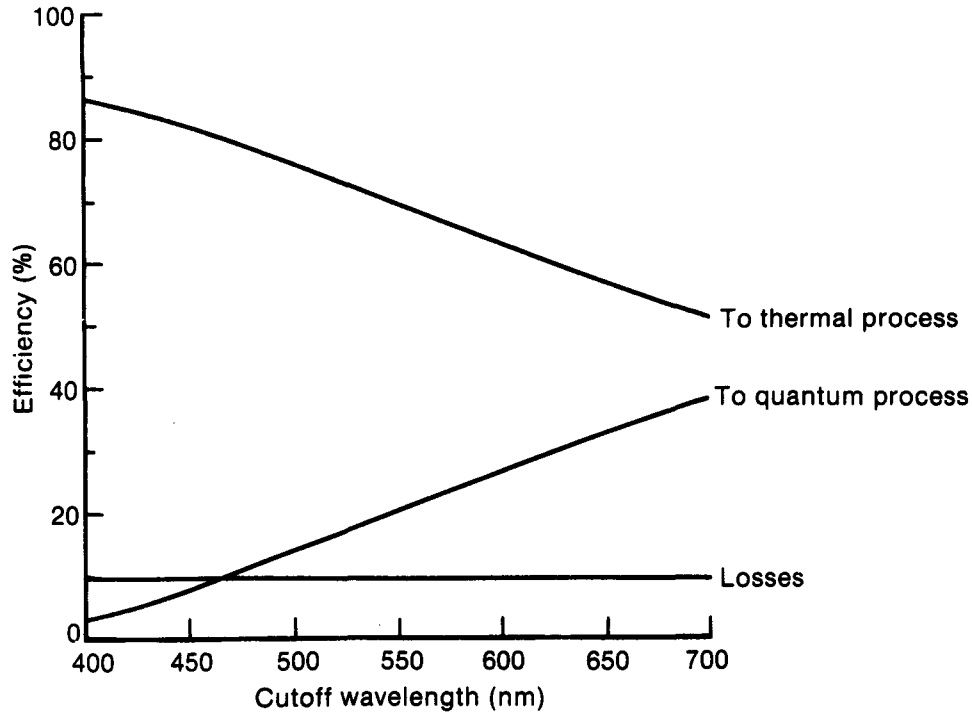

Figure 2-7. Results for an Ideal Holographic Concentrator

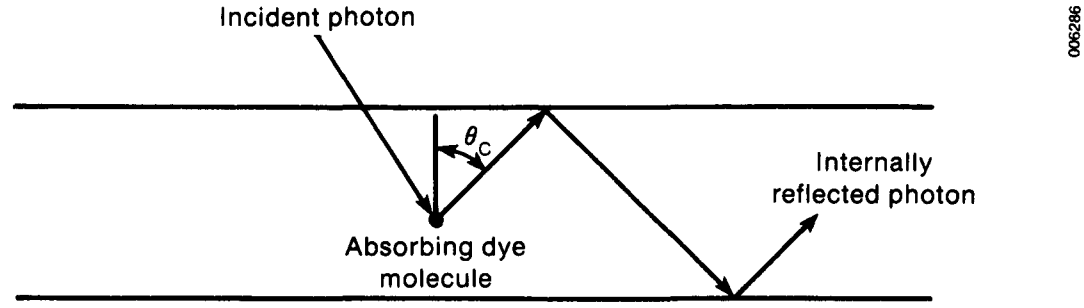

Figure 2-8. Absorption of an Incident Photon by a Fluorescent Planar Concentrator Showing the Critical Angle for Internal Reflection

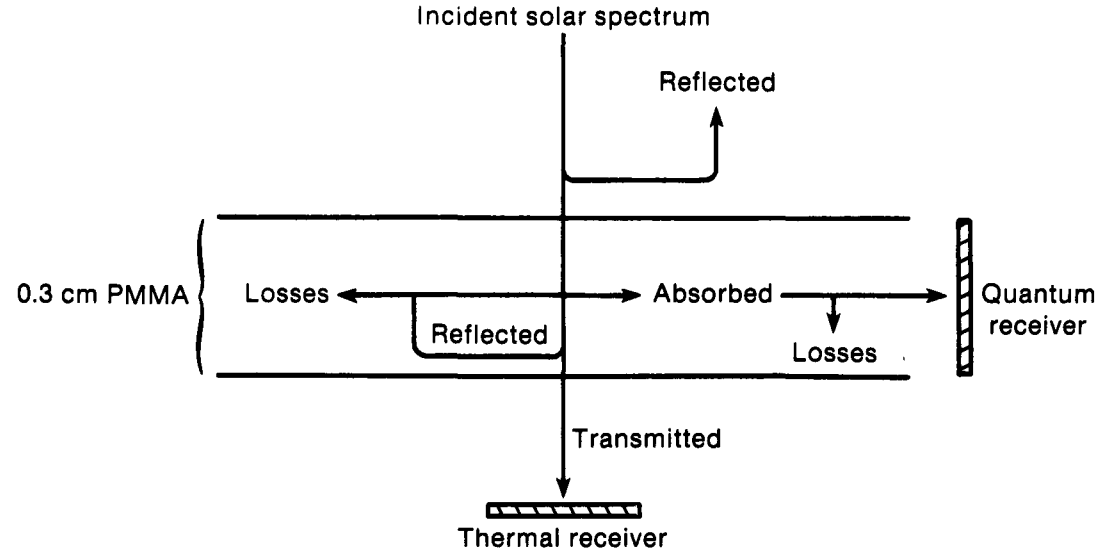

Figure 2-9. Model Used for a Fluorescent Planar Concentrator

As radiation strikes the top of the collector, a 4.0% reflection is assumed to occur. Of the remaining energy, a fraction is absorbed by the matrix and was determined from transmittance data for PMMA. Another fraction of the short wavelengths is absorbed by the dye. The energy remaining in the spectrum was then assumed to be transmitted to the thermal receiver, minus another 4.0% reflection loss that occurs at the second surface, again ignoring multiple reflections. This reflected component, at the bottom surface, consists of long-wavelength radiation, which was considered lost to both processes.

The fraction of solar radiation transmitted to the quantum receiver was calculated from the data shown in Table 2-1. These data give the current experimental efficiencies associated with the various loss mechanisms and efficiencies expected in the next few years with further improvements in the technology. The quantities are as follows: η_{abs} is the efficiency of absorption due to the absorption spectrum of the dye, η_{trap} is the efficiency of light trapping as determined by the critical angle for internal reflection, η_{qua} is the quantum efficiency of the dye, η_{stokes} is the Stokes efficiency (Stokes energy loss is $1-\eta_{stokes}$), η_{dye} is the efficiency of light conduction as limited by reabsorption of emitted light by the dye, and η_{mat} is a matrix efficiency ($1-\eta_{mat}$ gives the losses associated with matrix absorption, scattering, and internal reflection inefficiencies).

The results of this analysis are shown in Figure 2-10. The emitted wavelength, as opposed to the cutoff wavelength, indicates the wavelength at which the flourescent radiation is emitted. Care must be taken when comparing these results to the other efficiency curves; since the fluorescent radiation is nearly monochromatic, the entire energy of the photon is available for use.

Table 2-1. FPC Efficiencies

Parameter	Present Experimental Value	Value Expected in the Future
η_{abs}	0.205	0.29
η_{trap}	0.75	0.75
η_{qua}	0.95	1.00
η_{stokes}	0.75	0.75
η_{dye}	0.75	0.80
η_{mat}	0.90	0.95

Source: Goetzberger and Witter (1981).

Previously, the cutoff wavelength meant that photons with energy greater than the band gap are available; thus, the energy difference between the photon energy and the Gibbs energy of the quantum process is usually wasted. This shows up in the FPC analysis as the Stokes shift and was included in the results since it is an inherent part of the fluorescent process.

Data from only two dyes were available to generate the results of Figure 2-10 and correspond to the points at the end of the lines. The lines have not been extrapolated, because of the limited data available. The points have been connected by dashed lines, indicating that there is a large uncertainty.

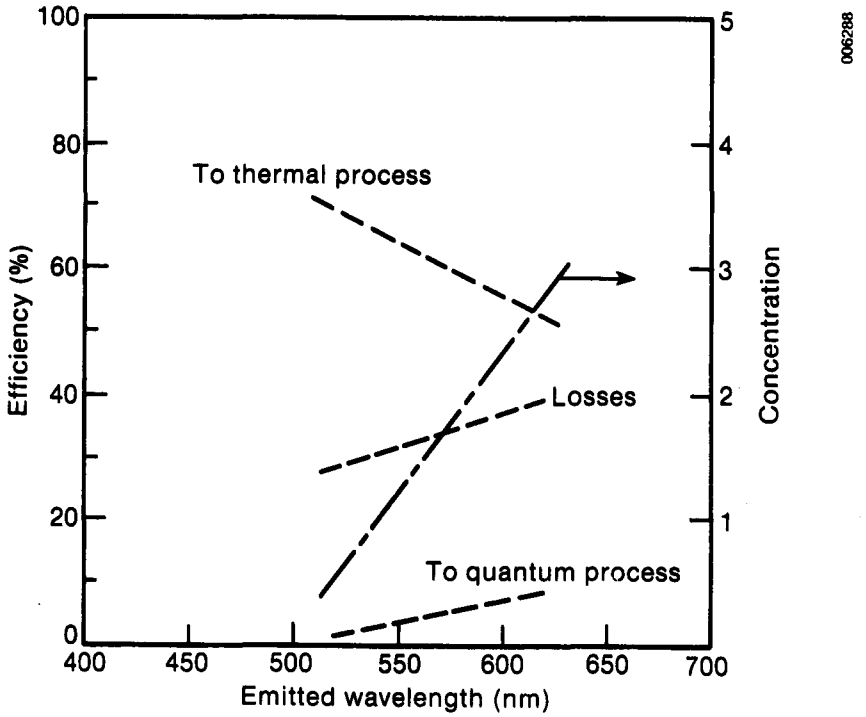

Figure 2-10. Results for an Experimental Fluorescent Planar Concentrator

The data for η_{abs} shown in Table 2-1 are for a dye that emitted close to 600 nm. The absorption by the other dye was estimated from an absorptance curve (Goetzberger and Witter 1981), and data for the other loss mechanisms shown in Table 2-1 were assumed to hold. Note that although absorption occurs in the near ultraviolet and blue portion of the spectrum, the quantum system will be limited to a smaller band gap because of the Stokes shift of the emitted radiation. Finally, all loss terms--absorption and reflection of both short- and long-wavelength components and the loss mechanisms associated with the dye and transport of radiation down the collector--have been combined into the single loss term shown in Figure 2-10.

Also shown is the concentration achieved by this collector geometry as a function of the emitted wavelength. The concentration is defined as the intensity of the emitted radiation at the edges of the collector divided by the intensity of a AM 1.5 sun. For example, a concentration of 1 means that the power emitted at the edges divided by the area of the edges equals a AM 1.5 sun. Concentration rises with increasing cutoff wavelength, since a larger fraction of the solar spectrum is collected.

Figure 2-11 shows the results of an analysis that used the more optimistic data of Table 2-1. Also, an antireflective coating on the top surface was added, which lowers the average reflectance to approximately 2.0%. The interesting point to notice is that only a small reduction in the overall loss is achieved. Instead, a larger amount of energy is available to the quantum system, but at the expense of energy available to the thermal system. This occurs because better absorption by the dye robs energy previously available to the thermal system; losses remain nearly the same, even though the efficiencies are greater because a larger amount of energy is available to be lost upon fluoresence.

A final point concerns the concentration that these devices are expected to achieve. As the size of the device is increased, a higher concentration would be expected, since a greater collection area is available. However, this also leads to lower overall efficiencies for the conduction of light to the edge of the collector, since the increased path length of the emitted radiation results in higher matrix losses. A recent analysis by Thomas et al. (1983) indicated that a concentration of 100 should be possible in the near future and that the theoretical limit is approximately 1000.

2.1.3 Comparison of Beam-Splitting Methods

A comparison of the various beam-splitting methods must consider the magnitude of the losses associated with each method. The fraction of energy available to either the quantum or thermal receiver is dictated by the band gap of the quantum process. But the most promising concepts will be those with the lowest losses, resulting in the maximum utilization of available energy. A comparison of the efficiency of the beam-splitting methods at 550 nm is given in Table 2-2, which rates the methods in order of increasing losses.

From the standpoint of maximum utilization of the available energy, selective absorption would appear to be ruled out. It has the highest losses of any other concept, but it also utilizes a greater portion of the shorter

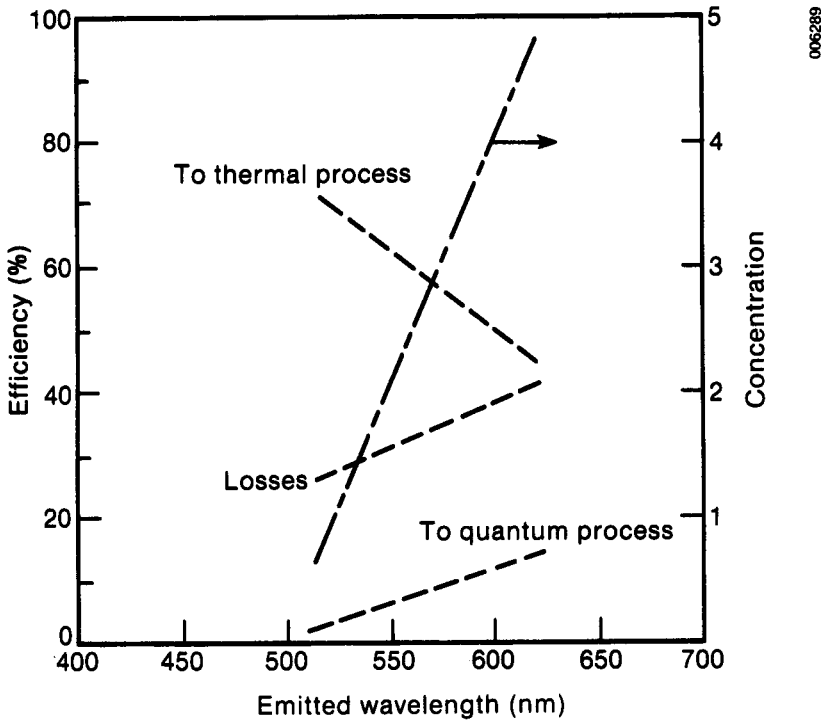

Figure 2-11. Results for an Ideal Fluorescent Planar Concentrator

wavelengths than most of the other concepts and is nearly equal to the ideal HC concentrator in this regard. Thus, this concept could be useful if a high-value product is produced by the quantum process.

When comparing FPC to the other concepts, a valid comparison can be obtained only by dividing the FPC results for the quantum process by 0.75, the Stokes shift efficiency. This gives a number comparable to the other processes by accounting for wasted photon energy above the band gap energy. This slightly raises the fraction of the energy to the quantum process and lowers the fraction loss (see Table 2-2). For the longer cutoff/emitted wavelengths, the losses from the FPC are high. Between 500 and 550 nm, these losses are comparable to the experimental values for HC. The main difference between the two concepts is that a larger fraction of the energy is available to the

Table 2-2. Comparison of Beam-Splitting Efficiency at 550 nm

Method	Losses (%)	Quantum Energy Available (%)	Thermal Energy Available (%)
HC (ideal)	10	20	80
Dichroic mirror	19	13	68
HC (experimental)	28	14	58
FPC (ideal)	28	9	63
FPC (experimental)	31	5	64
Selective absorption	42	19	39

quantum process from a HC. Conversely, a smaller fraction of the energy is then available to the thermal receiver. The optimistic case for the FPC displays the same trend, except that a slightly larger fraction of the energy is available to the quantum process due to slightly lower losses.

Dichroic mirrors display the next best utilization of the available energy. When compared with the experimental HC results, the fraction of the energy available to the quantum process is the same, but the difference in losses is made up by more energy available to the thermal process. The ideal HC has better performance than any of the other concepts, and when compared with the dichroic mirror, it has lower losses and a greater amount of energy available to both the quantum and thermal processes.

Dichroic mirrors and HCs are the two most promising techniques for splitting the solar spectrum for use by a hybrid quantum/thermal conversion system. They both have low losses and thus make very good use of available energy. The choice of beam splitters is not limited to the above devices, however, since system considerations and costs may dictate other choices. However, because these devices can achieve the best efficiencies, they are prime candidates for further consideration. The reader should note that many assumptions have been made in generating these results. The results are not meant to be absolute numbers but rather are intended to provide guidance in the selection of a beam-splitting device for a hybrid plant.

2.2 COLLECTOR DESIGN

Analysis of beam splitting has shown, as we noted earlier, that the most efficient devices are dichroic mirrors and holograms, even though at present many technical uncertainties are associated with the use of holograms for solar energy collection and concentration. With these two devices in mind, we designed a collector configuration to split the solar beam and be compatible with the central tower/receiver concept. In the following sections, we describe several designs that were considered before a holographic heliostat was finally selected.

2.2.1 Dichroic Mirror Concepts

A dichroic mirror in a central tower/receiver concept was considered in two designs: one concept is a double heliostat consisting of a dichroic mirror placed in front of and at a slight angle to the back reflective mirror on the heliostat, as shown in Figure 2-12. Light is split at the dichroic mirror surface, the reflected portion being sent immediately to one receiver on the tower. The other fraction passes through the dichroic mirror and is reflected from the back-mirrored surface back through the dichroic mirror to a second receiver on the tower. The angle between the dichroic and back mirrors separates the two beams, allowing each fraction to be collected at either the quantum or thermal receiver. The main disadvantages with this design are the extra optical losses associated with a second pass by the light beam through the dichroic mirror and the tracking requirements for a second mirror. Both of these factors are analyzed in Appendix A, which shows that another drive mechanism for the dichroic mirror is not needed. But the second pass by one

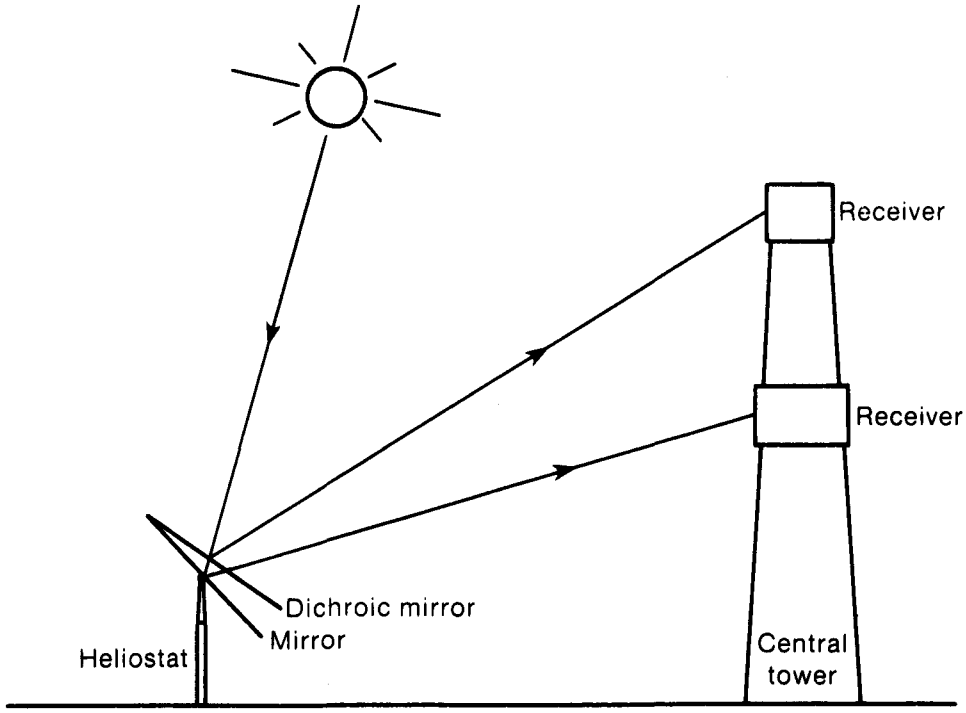

Figure 2-12. Dichroic Mirror Heliostat for Beam Splitting and Focusing

fraction of the solar beam back through the dichroic mirror results in increased losses: from 20% to 28% for a short-wavelength transmitting dichroic mirror and from 17% to 30% for a long-wavelength transmitting dichroic mirror. So, the dichroic mirror heliostat design was rejected.

The second design considered placing a dichroic mirror skirt around and on the tower to split the concentrated beam near the receivers. This design is illustrated in Figure 2-13. Concentrated sunlight from the heliostat field either passes through the dichroic mirror and is focused on the top receiver as normal, or the light reflected by the dichroic mirror is focused to a lower spot on the tower. The advantage of this method is that a smaller dichroic mirror area is required, a second pass by a light beam through the dichroic mirror is not needed, and additional tracking requirements need not be considered. The disadvantage is that the mirror would heat up because of the absorption of concentrated sunlight, and the performance of the dichroic coating would be uncertain. Another disadvantage is the great distance that the dichroic mirror must extend from the tower to catch the sunlight from the farthest heliostat. For instance, for a tower height of 80 m, a heliostat 350 m from the tower would require a dichroic mirror extending 45 m from the tower. The support and maintenance of a mirror this large was not considered to be a realistic alternative.

2.2.2 Holographic Heliostat

Another concept considered a holographic heliostat design, consisting of a holographic sandwich totally reflecting the incoming light. The reflector is manufactured in such a way that the shorter wavelengths up to the cutoff wavelength are reflected at a different angle than the longer wavelengths. This

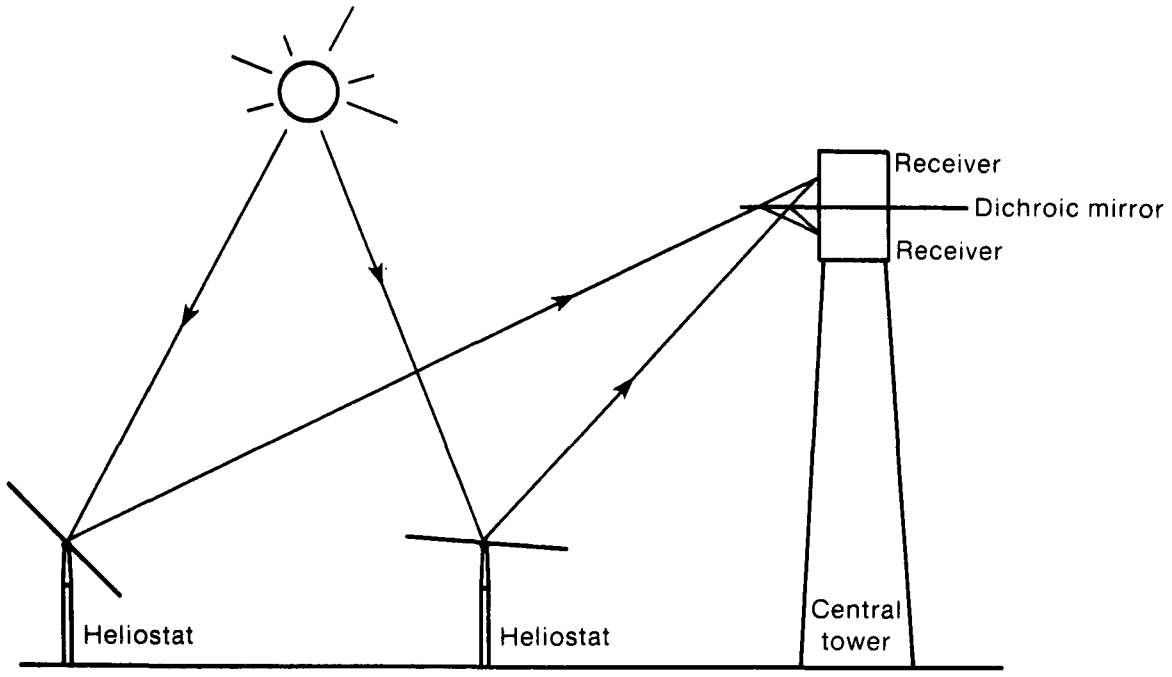

Figure 2-13. Dichroic Mirror Skirt for Beam Splitting of Concentrated Sunlight from the Heliostat Field

produces the two focus points on the tower in the same way that the dichroic mirror heliostat does (Figure 2-12). The holographic sandwich is covered with a thin glazing for protection and mounted onto a heliostat without the mirror. It is assumed that the normal heliostat steering equations applied and that no special tracking requirements are needed. The performance of the hologram is also assumed to equal the performance of a mirrored heliostat, independent of the chosen cutoff wavelength and the frequency of the light.

This last assumption is subject to much criticism and rebuttal, since the performance of holograms reflecting near 90% for even short wavelength-intervals (100 nm) is far from proven. Even theoretically, considering the expansion and swelling problems of holographic materials, it is doubtful that high efficiencies could be obtained in a broad enough wavelength band to cover the solar spectrum. Extending high reflection coefficients across the entire solar spectrum is realistically impossible. However, performance equal to that of a mirror was assumed to simplify the analysis and look at the limiting best case.

A more realistic design could be conceived in which a short-wavelength reflecting holographic sandwich is placed on top of the heliostat mirror and reflects at a slightly different angle than that of the mirror. Thus, the holographic sandwich would need to reflect a much smaller portion of the solar spectrum and would work at visible wavelengths where the majority of beam-splitting holographic work has been done. A possible advantage to this configuration is that the mirrored surface would be protected, but greater optical losses would occur at longer wavelengths due to the cover glazing and the transmission inefficiencies of the holograms.

SECTION 3.0

SYSTEMS ANALYSIS

In the following sections, a systems analysis of a hybrid quantum/thermal plant for hybrid production is presented. These results are compared with results for a base-case thermal plant producing hydrogen by an electrolysis process. This allows the relative merits of the hybrid plant to be determined. A simple analysis of caprolactam production from a hybrid plant is also presented. Because caprolactam can be produced photochemically, it is a candidate for a hybrid plant.

3.1 HYDROGEN PRODUCTION

Hydrogen production was selected as a means for comparing a thermal process with a hybrid quantum/thermal process. The thermal-only plant generates hydrogen by an electrolysis process from electricity obtained from a Rankine-cycle energy conversion system using molten salt for storage. The quantum process chosen generates hydrogen by means of a photoelectrochemical process. The thermal part of the hybrid plant uses the same conversion cycle as the thermal-only plant. Hydrogen production from both the thermal and the quantum process was chosen because it provides a basis for comparing both plants.

The use of hydrogen as a fuel has been thoroughly investigated and demonstrated. Hydrogen is a high-heating-value fuel that burns easily and cleanly and could have a major impact in the energy marketplace. The problem is that hydrogen production technology is not at a stage of development that would make it competitive with other energy sources.

If a quantum process is to make a significant impact on the cost of producing a fuel, it must be both cheaper than alternative processes and must use a significant portion of the solar spectrum. Thus, a photoelectrochemical process for direct hydrogen production was chosen, because it is a potentially cheap process that uses short-wavelength photons directly to produce hydrogen and oxygen. Higher efficiencies may be obtained because a thermal-to-electrical energy conversion step is eliminated. Also, since some of the available solar energy is directed to the quantum process, less energy is available to the thermal process compared with the base case, which results in a reduction in size of the thermal and electrolysis plants for the same total hydrogen production rate. The advantages of the hybrid system will be determined by the trade-offs between, on the one hand, the efficiencies and cost of the photoelectrochemical receiver and, on the other, the credits for reducing the size needed for the thermal and electrolysis plants.

Hydrogen production also has the advantage of potentially using a large fraction of the solar spectrum. The theoretical photon energy required to drive the water dissociation reaction is 1.23 eV. This corresponds to a band-gap wavelength of nearly 1000 nm, which covers about 70% of the available energy in the spectrum. However, only 46% of this energy can be used, and second-law considerations reduce the useful energy even further.

3.1.1 System Description

3.1.1.1 The Base Case

The base-case thermal electric hydrogen-producing plant is shown in Figure 3-1 and consists of six major components: the heliostat field, the thermal receiver, thermal storage, a heat exchanger, a Rankine-cycle power plant, and the electrolysis plant. This system is based upon the central receiver design and specifications of Apley et al. (1980) and Laity et al. (1980) for a 100-MW_e solar thermal plant. A 100-MW_e plant was selected because this is the size of central receiver plants for producing hydrogen that are now being investigated (see Bilgen and Bilgen 1984, Hammerli 1984, and Bilgen and Bilgen 1982).

The plant is a single tower/receiver design having an overall solar energy to electricity conversion efficiency of 16.8%. The output is 100 MW_e, using the optimum design conditions given by Apley et al. (1980) of approximately 2800 kWh/m^2-yr direct normal solar flux. The efficiencies of each of the subsystems will be presented in Section 3.1.2.1.

Heliostat and Receiver Subsystems. The heliostat field consist of approximately 25,500 49-m^2 heliostats having a total collection area of 1,250,000 m^2. The receiver is a cavity type operating at 538°C with a molten draw salt as the heat transport media. The concentration on the thermal receiver is 300 suns.

Thermal Storage/Rankine-Cycle Power Plant. The Rankine cycle heat engine is a conventional steam power generation cycle consisting of a turbine, a generator, a condenser, a pump, and associated auxiliary equipment. Steam is generated by the heat exchanger from hot molten salt at 538°C. The hot molten salt comes either directly from the receiver during normal operation or is pumped from the storage reservoir at night.

Electrolysis Plant. Several prospective electrolysis techniques were reviewed (see Bonner et al. 1982, Ficket and Kalhammer 1977, Nutall and Russell 1979, Russell 1981, and Beller and Mezzina 1983) before the General Electric Solid Polymer Electrolyte (SPE) electrolysis process was selected for use. The SPE process consists of a perfluorinated polymer membrane (NaFion®) to which sulfanate groups are attached, giving the membrane its ion exchange and hydrogen ion conduction properties. Small amounts of platinoid metal catalyst are attached to both sides of the membrane to form the anode and cathode, and these are sandwiched between current collection screens, completing the basic cell structure. The individual cells are then joined in series to form electrolyzer stacks. The demonstrated efficiency of this device is 77% with a 1.90-V applied potential at a high current density of 1076 mA/cm^2. In this study, a goal of 85% stack efficiency will be assumed (Bonner et al. 1982).

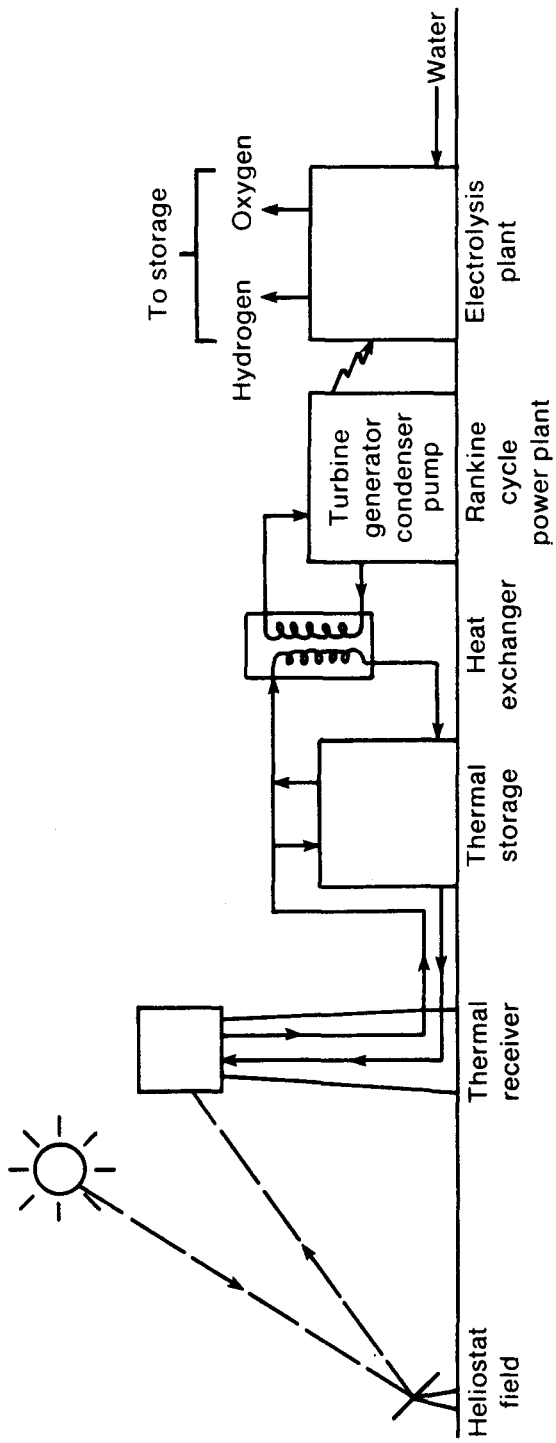

Figure 3-1. Solar Thermal Electric Hydrogen Production

3.1.1.2 Hybrid Quantum/Thermal System Description

The hybrid quantum/thermal system configuration is shown in Figure 3-2. Sunlight is split by the holographic heliostat into the long-wavelength and short-wavelength components and collected by the appropriate receiver. A design for a quantum receiver has been conceived from a known photoelectrochemical process. An additional requirement of cooling water is needed by the hybrid system to maintain the photoelectrochemical receiver near ambient temperature.

Thermal System. The details of the thermal portion of the hybrid system have been left out in Figure 3-2, but are the same as the thermal electric plant of Figure 3-1. The only difference is that all components have been scaled down in size to accommodate the reduction in energy input to the thermal process. We have assumed improved heliostat tracking and optics, so that the same solar thermal receiver temperature as the base case plant will be maintained on the smaller thermal receiver.

Quantum System. The photoelectrochemical process chosen to perform the electrolysis is based on the recommendations of Parkinson (1984) and several references in the area of solar-assisted water electrolysis (Nozik 1981, Gratzel 1981). The process would use two separate electrodes: hydrogen is produced on the illuminated cathode and oxygen evolved on the dark anode. This arrangement ensures that explosive hydrogen/oxygen mixtures will not have to be handled.

The cathode consists of a p-type semiconductor (e.g., GaAs/P) deposited as a thin layer on a conducting substrate; a catalyst (platinum) is also needed to initiate the reaction. Upon irradiation, hydrogen is produced from an acidic solution. At the same time, the dark anode (e.g., RuO_2, TiO_2) produces oxygen. The cathode and anode solutions are separated by an ion conduction membrane. NaFion®, used in the General Electric SPE Electroylzer, is the best candidate material.

A concept for the photoelectrochemical receiver is that the anode and cathode would be on concentric cylinders inside a glass tube, as shown schematically in Figure 3-3. The acidic solutions would flow up and around the electrodes, removing the gases as they are produced. We have assumed that the flow rate will be sufficient to remove small bubbles as they form from the cathode, so that gas evolution will not reduce the amount of light illuminating the cathode. The central tower would be ringed with these glass tubes vertically placed. A pump and header arrangement would supply the tubes with the acid solution. At the top of the glass tubes, the gases would be separated from the liquid and stored, and the acid solution would be recirculated through a heat exchanger (cooler) to remove the excess heat. The conceptual design has been used only as a basis for cost-estimating.

To determine the operating characteristics (cutoff wavelength, efficiency, etc.) of the photoelectrochemical receiver, it is necessary that photoassisted water electrolysis be theoretically analyzed. Laboratory studies of photochemical and photoelectrochemical water decomposition have resulted in low

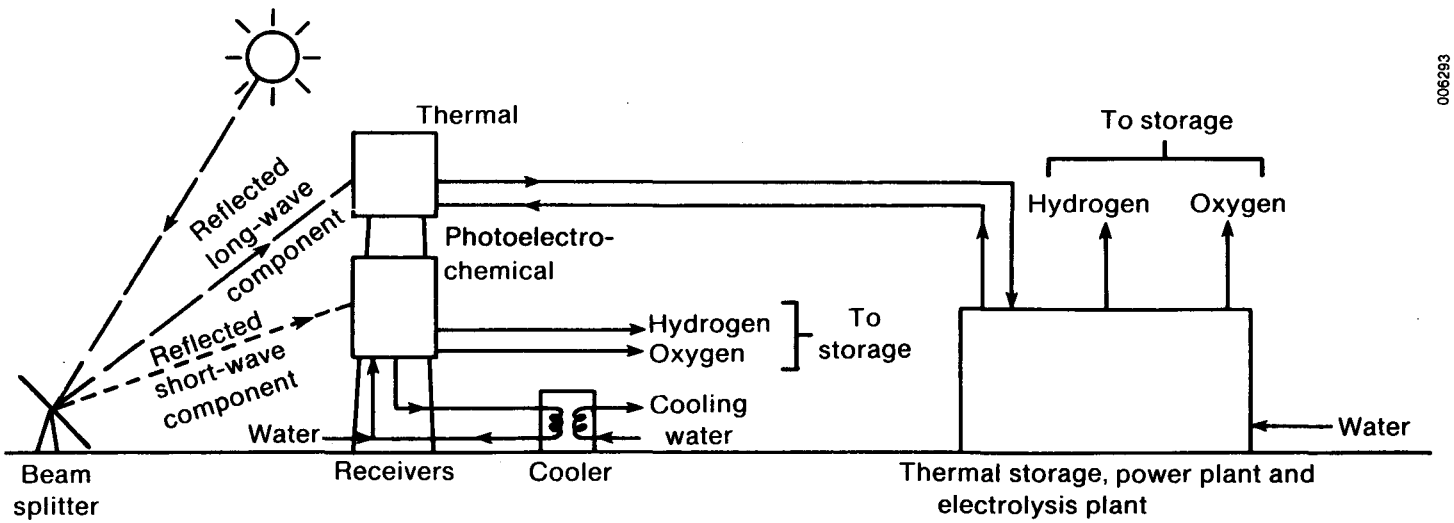

Figure 3-2. Dual Hydrogen Production System: Solar Thermal Electric plus Photoelectrochemical

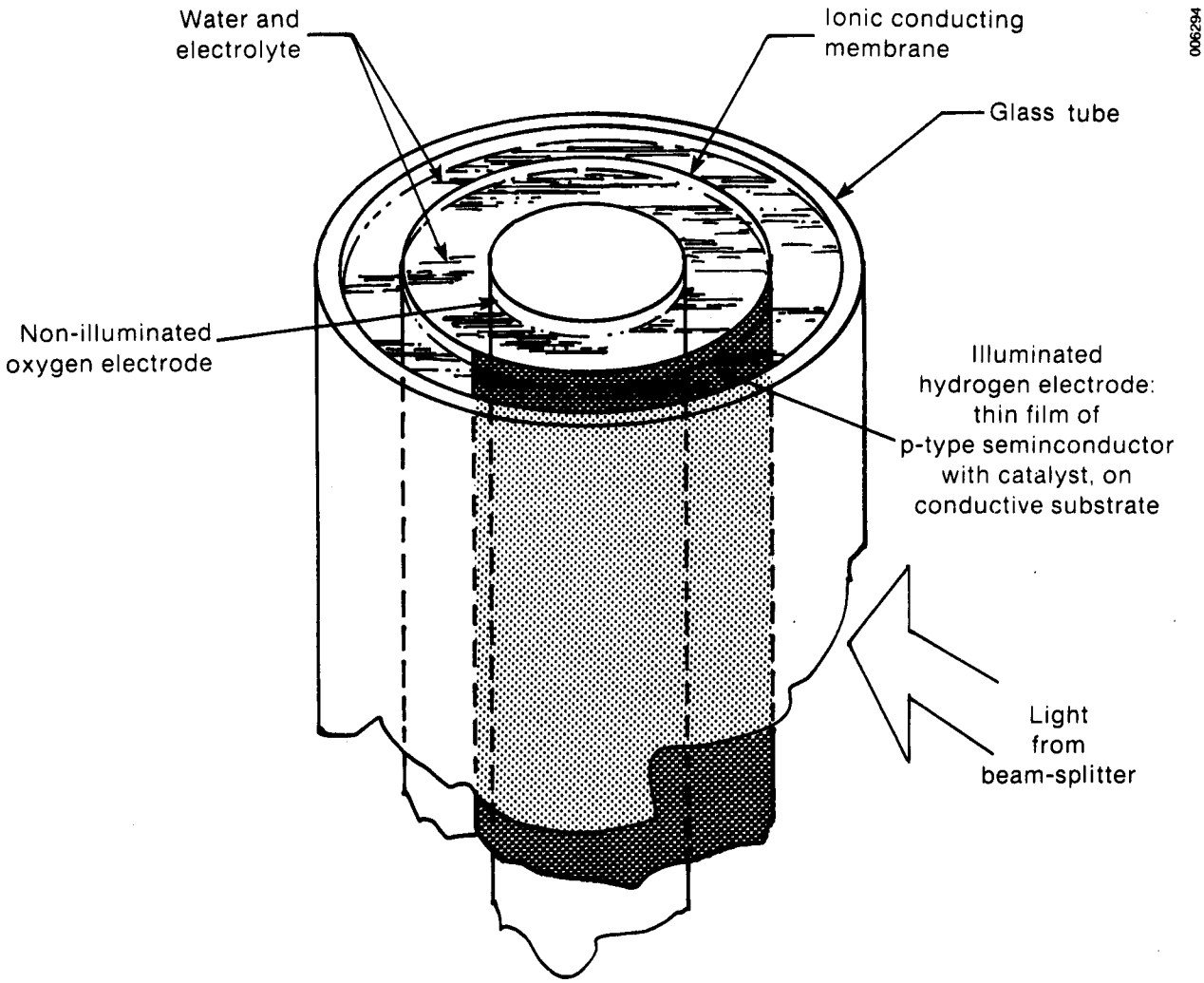

Figure 3-3. Schematic Diagram of Photoelectrochemical Receiver

overall conversion efficiencies (<1%) for the solar spectrum (Biddle and Peterson 1983). The highest efficiency reported to date for a photochemical process is 12% for splitting hydrogen chloride into hydrogen and chlorine. The maximum theoretical efficiency for a single electron quantum process depends on the receiver temperature and wavelength of light used, but it is close to 31% for the entire solar spectrum at 300 K (Haught 1984).

The flux level or solar concentration is also an important operating parameter needed to determine efficiency and receiver size. Parkinson (1984) suggested that 200 mA/cm^2 is the maximum current density at which the photoelectrochemical process would operate efficiently. We have made the optimistic

assumption that with further improvements, a photoelectrochemical process will operate with a current density more comparable to SPE electrolysis. Arbitrarily using a solar concentration factor of 100, a quantum efficiency of 0.8, and prior knowledge of the approximate cutoff wavelength, and assuming one photon generates one electron, the current density is approximately 700 mA/cm^2. The quantum efficiency is the fraction of available photons that produces an electron.

The technique used to determine efficiency is based on Haught's (1984) method. The theoretical photon energy required to split water is 1.23 eV, corresponding to the Gibbs free energy. However, no water decomposition reaction can operate with photons of this wavelength. At present, photoelectrochemical processes require 2.2-eV photons to work (Biddle and Peterson 1983). We have again made the optimistic assumption that the reaction can be driven by 1.75-eV photons. Using this as the required band-gap energy and a solar concentration of 100, the analysis gives 620 nm as the required cutoff wavelength and a conversion efficiency of 21%. An additional efficiency factor is required that converts photon energy to the chemical energy of the hydrogen (85%). This is the ratio of the enthalpy increase (1.48 eV) of the hydrogen to the required bandgap energy (1.75 eV). Finally, the overall conversion efficiency is the product of 21%, the chemical efficiency, and the quantum efficiency, giving 14%.

Since these assumptions regarding the photochemical process are quite optimistic, a sensitivity analysis was performed using different operating parameters. The parameters used are shown in Table 3-1; the design basis so far discussed in the text is for the optimistic case. For other cases, the cutoff wavelength was lowered, thus reducing the available energy to the quantum process (fraction of energy in solar spectrum at less than the cutoff wavelength), although the required potential is still 1.75 eV. The current density was lowered, effectively increasing the size of the photoelectrochemical receiver, and the quantum efficiency has also been lowered.

Table 3-1. Photoelectrochemical Process Operating Parameters

Parameter	Design Basis		
	Optimistic	Moderate	Pessimistic
Cutoff wavelength (nm)	620	600	580
Conversion efficiency	0.21	0.18	0.17
Current density (mA/cm^2)	700	450	200
Quantum efficiency	0.8	0.65	0.5
Chemical efficiency	0.85	0.85	0.85
Photoelectrochemical process overall efficiency	0.14	0.10	0.07

3.1.2 Performance Comparisons

The following sections present a comparison of efficiencies and costs for a thermal/electric versus a hybrid quantum/thermal hydrogen-producing plant. Details of the design basis and a breakdown of the component cost and efficiencies are provided.

3.1.2.1 Process Efficiencies

The conversion efficiencies used in this study are shown in Table 3-2 for both hydrogen-producing processes, assuming that 100% of the energy in the solar spectrum is available. All data for the thermal conversion steps are from Apley et al. (1980), except for data on the electrolysis plant, which are from Bonner et al. (1982). The photoelectrochemical process efficiency is taken from Table 3-1 for the optimistic case. The same field efficiency has been used for the photoelectrochemical step and assumes that the beam-splitting and reflection ability of holograms is equal in performance to that of a mirror. Also, a 90% photoelectrochemical receiver efficiency has been assumed to represent the fraction of light incident on the receiver that is absorbed by the semiconductor.

A schematic representation of the energy path for hydrogen production for a thermal/electric plant is shown in Figure 3-4a, which depicts the large energy losses that occur at the heliostat field and during the thermal-to-electrical energy conversion step. The field losses are a result of poor optics, cosine losses, inaccurate heliostat tracking, and blocking and shading of adjacent heliostats. This type of loss is common to both plants and cannot be avoided. Other losses from the receiver, from transmitting and storing hot molten salt, and electrical losses from the electrolyzer are minor, but they do reduce the overall hydrogen production efficiency to 14%.

Table 3-2. Conversion Efficiencies for the Thermal and Photoelectrochemical Conversion Steps[a]

Parameter	Thermal Conversion	Photoelectrochemical Conversion
Field efficiency	0.461	0.461
Receiver efficiency	0.950	0.900
Transmission and storage	0.985	--
Conversion to electricity	0.383	--
Photoelectrochemical process	--	0.140
Electrolysis plant	0.850	--
Overall conversion efficiency to hydrogen	0.140	0.058

[a]Assumes 100% of the energy in the solar spectrum is available to each process.

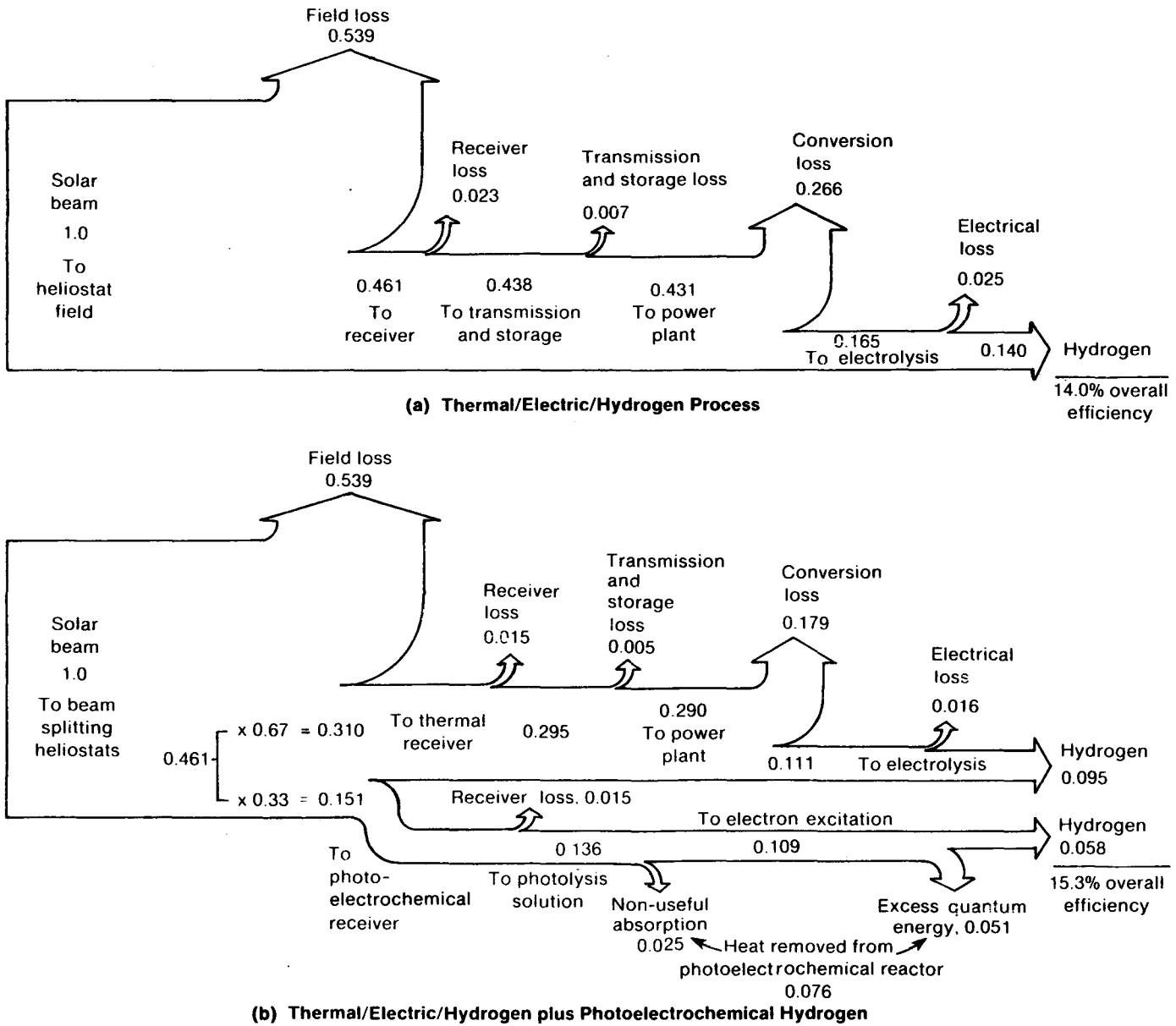

Figure 3-4. Energy Paths for Hydrogen Production. Numbers are fractions of energy in solar beam.

In Figure 3-4b the energy path for the hybrid plant is shown. Again, 53.9% of the total energy is immediately lost at the heliostat field, and the rest is directed to the thermal and photoelectrochemical receiver. The amount of energy diverted to each receiver depends on the chosen cutoff wavelength and is 33% to the photoelectrochemical receiver and 67% to the thermal receiver, in the optimistic case. The thermal side of the plant converts 9.5% of the available energy to hydrogen energy (0.14 times 0.67, the fraction of solar energy directed to the thermal receiver). On the photoelectrochemical side, losses occur as a result of receiver inefficiency, unutilized photons as given by the quantum efficiency of 80%, and the theoretical excess energy available from the photons. The photoelectrochemical side converts 5.8% of the available energy to hydrogen energy, and the overall conversion efficiency is 15.3%, which is higher than the thermal/electric plant because of the greater efficiency at which the photoelectrochemical process converts photon energy to hydrogen energy. This is the result of having eliminated the large energy loss associated with electrical-to-thermal energy conversion.

3.1.2.2 Economic Results

The design output capacity for the base-case thermal plant is 100 MW_e. This corresponds to 85 MW_e of equivalent hydrogen output because of the efficiency of the electrolysis plant. This same hydrogen output rate is the design basis for the hybrid plant. Because of the increased overall efficiency of the hybrid process (15.3%, compared with 14.0% for the base-case plant), the heliostat field can be smaller for the hybrid plant than for the thermal-only plant to accomplish the same hydrogen production rate. The sizes of key components for the base-case plant and for the three design bases for the hybrid plant are given in Table 3-3. The size of components for the base-case plant was taken from the optimum 100-MW_e design of Apley et al. (1980).

The heliostat mirror area required for the hybrid plants was calculated from a ratio of the overall conversion efficiencies. The thermal power plant and thermal storage requirements were calculated based on the reduced amount of energy to the thermal receiver and the ratio of the mirror area of the hybrid plant to the mirror area of the base-case plant. The photoelectrochemical receiver area was calculated from the allowed current density, as given in Table 3-1, based upon the concentration factor of 100. The cooler area was estimated from the amount of heat that needs to be rejected from the photoelectrochemical receiver. Hydrogen production from the photoelectrochemical receiver was calculated from the theoretical conversion efficiency, receiver and field efficiencies, and the amount of energy available to the receiver. Electrolysis plant hydrogen production was based on electrolysis efficiency and thermal plant size.

Component Cost Estimation. Unit cost data for key system components are presented in Table 3-4, with the source of the information referenced. It is assumed that the cost of the beam-splitting heliostats are the same as the standard heliostats. This is a reasonable estimate as a limiting case. Dichroic mirrors would add to the cost of the heliostat, but holograms are a possible low-cost alternative that could replace the mirror, thus making the heliostat cheaper. Details of the photoelectrochemical reactor cost estimate

Table 3-3. Key Size Parameters for the Base-Case Thermal Plant and for the Three Design Bases of the Hybrid Plant

Parameter	Base-Case Plant	Design Basis of the Hybrid Plant		
		Optimistic	Moderate	Pessimistic
Heliostat mirror area (10^6 m^2)	1.25	1.14	1.22	1.30
Thermal receiver area (10^3 m^2)	4.2	2.6	2.9	3.2
Photoelectrochemical process:				
Receiver area (10^3 m^2)	--	3.6	4.6	7.9
Cooler area (10^4 m^2)	--	1.1	1.2	1.2
Hydrogen production (10^4 SCMH)	--	.9	.8	.5
Thermal storage (GWh_t)	3.7	2.3	2.5	2.8
Power plant (MW_e)	100	62	68	76
Electrolyzer hydrogen production (10^4 SCMH)	2.4	1.5	1.6	1.9
Total hydrogen production (10^4 SCMH)	2.4	2.4	2.4	2.4

Table 3-4. Unit Costs of Major System Components

Item	Unit Cost (1980 $)	Source
Heliostats:		
Standard	$97/m^2	Apley et al. (1980)
Beam splitting	$97/m^2	Assumed
Central receiver equipment:		
Thermal receiver	$2800/m^2	Apley et al. (1980)
Photoelectrochemical receiver	$2324/m^2	Appendix B
Tower	$12 to $32 x 10^6 each	Apley et al. (1980) with assumptions
Photoelectrochemical cooler	$300/m^2	Peters and Timmerhaus (1980)
Transport	$12 x 10^6/100 MW_e	Apley et al. (1980)
Storage	$12 x 10^6/100 MW_e (12-h storage)	Apley et al. (1980)
Power plant	$31 x 10^6/100 MW_e	Apley et al. (1980)
Electrolysis plant	$250/kW	Bonner et al. (1982)
Balance-of-plant	11% of total of all of above	Apley et al. (1980)
Indirects	25% of total of all of above	Apley et al. (1980)

are given in Appendix B, showing a cost only 17% lower than the thermal receiver, so it seemed to be a reasonable estimate. Scaling of capital investments to different sizes was done assuming constant unit costs, except for the tower. This is reasonable for items such as the heliostat field and the electrolysis plant, but may be somewhat in error for other items (e.g., storage and transport). Large-scale, single-unit items (e.g., tanks) tend to scale to a power of less than 1 (0.6 to 0.7) (Peters and Timmerhaus 1980). However, the error associated with such scaling is small compared with total plant cost and probably does not contribute significantly to the trends presented.

Tower cost for the base case was estimated by knowing the total central receiver tower cost and subtracting the receiver cost determined from a cost graph. No information on tower only cost was provided, except as a function of tower height. Adding a photoelectrochemical receiver to the tower means that further structural support will be necessary. Also, a greater tower height might be necessary if performance is to be preserved. Estimating the additional height needed would require guessing at the dimensions of the receiver, but added costs arising from the additional weight were not known. Since not enough information was available to determine the tower cost, it was estimated by multiplying the cost of the tower for the base case by the ratio of both receiver areas for the hybrid plant to the thermal receiver area for the base-case plant.

Hydrogen Production Cost. Estimates of capital investments in millions of (1980) dollars and hydrogen cost are shown in Table 3-5 for the base-case plant and for the three design bases for the hybrid plant. Note that balance-of-plant costs were estimated to be 11% of the sum of all items listed above it in the table and indirect costs as 25% of the sum of all the items listed above it. The cost of hydrogen production was estimated using an annual fixed-charge rate of 0.157 of the initial investment and levelized operation and maintenance cost of 0.017 of the initial investment; this and other economic assumptions are given by Apley et al. (1980). Thus, total levelized annual costs are 0.174 times the initial investment; this divided by the annual energy content of the hydrogen product gives the cost in $/GJ. The results show that an approximate 10% decrease in hydrogen production cost can be achieved with the optimistic hybrid plant.

A comparison with other, similar studies shows similar economic results. Bilgen and Bilgen (1984) projected costs of about $36/GJ for hydrogen produced by a solar central receiver/SPE electrolysis process for similar conditions. For solar-photoelectrochemical hydrogen production, Biddle and Peterson (1983) obtained $34/GJ with flat-plate collectors assuming a 10.3% conversion efficiency and $94/GJ for a concentrating parabolic system with an 11.6% efficiency. This study assumed a fixed-charge rate and operating and maintenance (O&M) costs of 22%. Thus we see that values obtained in the present study are lower than other estimates but do not seem to be unreasonable.

Sensitivity Analysis. The data shown in Tables 3-1 and 3-5 illustrate the sensitivity of the economic results to assumptions regarding the performance of the photoelectrochemical process. As performance assumptions change from

Table 3-5. Investment Estimates and Cost of Hydrogen Production (millions of 1980 dollars)

Item	Base-Case Plant	Hybrid Plant Design Basis		
		Optimistic	Moderate	Pessimistic
Heliostat field	121	111	118	126
Central receiver equipment:				
Thermal receiver	12	7	8	9
Photoelectrochemical receiver	--	8	11	18
Tower	12	18	21	32
Photoelectrochemical cooler	--	4	4	4
Transport	12	7	8	9
Storage	12	7	8	9
Power plant	31	17	21	24
Electrolysis plant	25	16	17	19
Balance-of-plant	25	21	24	28
Indirects	62	54	60	70
Total capital investment	312	270	300	348
Hydrogen production cost ($/GJ)	30	26	29	33

optimistic to pessimistic, the economic results shift from favorable to unfavorable, compared with the base-case plant, although even the pessimistic assumptions are optimistic compared with those demonstrated so far in the laboratory.

Lowering the quantum efficiency, the receiver current density, and the fraction of energy available to the quantum process will most strongly influence the economic results. All of these factors directly influence overall process efficiency and the photoelectrochemical receiver size required, which, in turn, affects all other costs and size requirements. Another factor influencing the results is beam-splitting efficiency, but a sensitivity analysis was not performed on this variable. Even if holograms cannot function at the efficiencies of mirrors, dichroic mirrors still have relatively high efficiencies, as indicated by the analysis in Appendix A, and they could replace holograms (although costs were not determined).

3.1.3 Conclusion

The results show that a 13% decrease in hydrogen production cost is possible and that both the maximum theoretical efficiency and highly optimistic current densities for the photoelectrochemical process are required. It is more reasonable to expect that the assumptions of the moderate design are achievable, but no significant improvement in cost accompanies that design, compared with the base-case plant. Thus, there is little economic incentive to construct a hybrid plant utilizing a photoelectrochemical process for hydrogen productions. However, the same conclusion does not apply to all hybrid processes, as we see in Section 3.2, which investigates the use of a hybrid system for production of the chemical caprolactam.

3.2 CAPROLACTAM PRODUCTION

Caprolactam (2-oxohexamethyleneimine) is a chemical that has been commercially produced using a photochemical process. Although there are other chemical routes for caprolactam production, Toyo Rayon Co. in Japan is still using the PNC (photonitrosation of cyclohexane) method, and until a few years ago, they still claimed that the PNC process was competitive with other traditional production methods (European Chemical News 1976). Other early work showed that the PNC process has production cost mid-range between some of the more traditional and newly developed processes for caprolactam production (Taverna and Chiti 1970). The idea to use a hybrid system for caprolactam production was suggested by V. K. Mathur of the University of New Hampshire, a faculty participant at SERI during the summer of 1984. Mathur, who has provided more details on this process (1985a), performed a general engineering analysis which was completed after the SERI work.

This section should provide a rough estimate of the production cost of caprolactam in a hybrid plant; a detailed cost and engineering analysis, however, is beyond the scope of this study. The caprolactam production process is uniquely suited to a hybrid plant because many of the processing steps require thermal energy inputs. This analysis is concerned with determining the replacement cost of substituting photons from a mercury lamp with solar photons.

3.2.1 Process Description

The photochemical reaction that converts cyclohexane to cyclohexanone oxime hydrochloride is an intermediate step in the production of caprolactam. The major processing steps consist of first burning ammonia in air to produce nitrogen oxides; this is combined with sulfuric acid to form nitrosyl sulfuric acid. Then hydrogen chloride is introduced into the nitrosyl sulfuric acid, producing a gaseous mixture of nitrosyl chloride and hydrogen chloride. This is introduced into the photochemical reactor with liquid cyclohexane present, where conversion to cyclohexanone oxime hydrochloride takes place. This product is then treated with oleum, producing caprolactam by Beckman rearrangement. Steam is needed for various product recovery and recirculation stages. More details on the process and the photoreactor are given by Hulme and Turner (1967) and Ito and Matsuda (1969).

3.2.2 Caprolactam Production Analysis

The following sections present the methods used to determine the cost of solar photons versus the cost of photons from a mercury lamp and compare the results in terms of the cost of caprolactam production. The analysis draws on the efficiencies and plant sizes used in regard to the hydrogen-producing hybrid plant.

3.2.2.1 Methods and Results

To determine solar photon cost, it was first necessary to determine the caprolactam production rate per photon. This was done using the referenced experimental data shown in Table 3-6. Multiplying energy consumption by the photon production rate yields the number of photons used. Then, assuming an electricity cost of $0.10/kWh, the photon cost and electricity cost can be calculated.

From the number of photons used per kg of caprolactam produced (2.80×10^{24} photons/kg), production from the hybrid plant can be calculated. Because this number was calculated from a known power consumption rate for the process, it inherently includes inefficiencies and does not represent a theoretical conversion efficiency. Before the production rate can be calculated,

Table 3-6. Production Costs for the PNC Process

Energy consumption[a]	2.5 kWh/kg
Photon production rate[a]	2.1×10^{24} photons/kWh
Photons used	5.25×10^{24} photons/kg
Photon cost[b]	2.1×10^{24} photons/$
Electricity cost[b]	$0.25/kg

[a]Source: Fischer 1976.
[b]Assumes $0.10/kWh.

it is necessary first to calculate the number of solar photons available for the plant. Using the yearly averaged solar flux assumed for the 100-MW_e plant of 2800 kWh/m^2, a daily average of 661 cal/cm^2 was calculated and compared with the normal AM 1.5 irradiance standard of 0.018 cal/cm^2-s given by Matson et al. (1981). From these numbers, the yearly average number of hours per day of irradiance available was calculated as 10.2 h. From the standard 1.5 AM spectrum, the number of photons available from 365 to 540 nm was also calculated. This was converted to number of photons available per hour and on a yearly basis using the heliostat area and the field and receiver efficiencies. This information is summarized in Table 3-7.

From the number of photons necessary to produce a kg of caprolactam (Table 3-6) and the number of photons available per year from the hybrid plant (Table 3-7), the production rate and cost of solar photons from the hybrid plant can be determined. The cost was estimated in the same way as that of hydrogen production, by multiplying 0.174 times the initial investment. Instead of separating out the cost of short-wavelength photons, we used the total capital investment for the optimistic hybrid plant presented in Section 3.1.2.2, which includes the cost of supplying thermal energy. This assumes that the thermal portion of the plant can supply all the energy and power needs for the entire plant. A caprolactam production plant will cost less to build and start up than the hydrogen production plant because the electrolyzer can be eliminated and thermal power plant size significantly reduced; steam could be generated directly in the thermal receiver and used in processing the caprolactam. However, an initial capital investment of $276 million was considered adequate, as a more accurate number would require a more detailed design and systems study. Because of uncertainty in the cost of the caprolactum plant, the $276 million was assumed to represent 1984 dollars. The results are summarized in Table 3-8.

3.2.2.2 Comparison of Results

Table 3-9 summarizes the results and shows current price and production information. Remember that photon and production costs include total cost minus raw material cost for the hybrid plant compared with only electricity cost for

Table 3-7. Photons Available for Caprolactam Production from Hybrid Plant

Solar irradiance (365 to 540 nm)	3.52×10 photons/m^2-s
Heliostat field area	1.25×10^6 m^2
Field efficiency	46%
Receiver efficiency	90%
Useful photons	6.55×10^{29} photons/h
Number of operating days	300 days/yr
Number of operating hours	10.2 h/day
Total available photons	2.00×10^{33} photons/yr

Table 3-8. Solar Photon Cost for Caprolactam Production in Hybrid Plant

Total available photons (from Table 3-7)	2.00×10^{33} photons/yr
Photons actually used (from Table 3-6)	5.25×10^{24} photons/kg
Production rate	3.81×10^{8} kg/yr
Annualized fixed change rate plus O&M	0.174
Initial investment	$\$276 \times 10^{6}$
Photon cost	4.16×10^{25} photons/$
Production cost	$0.126/kg

the PNC process. Electricity and photon costs are higher for the PNC process even when thermal requirements have been included in the cost from the hybrid plant. Even though raw material cost with by-product credits is approximately half the production cost (Taverna and Chiti 1970), a significant reduction in caprolactam cost can be achieved with the hybrid system.

Of interest is the current production rate (1983) for the United States, which is only slightly greater than the production from one 100-MW_e-sized hybrid plant. Although caprolactam could be more cheaply produced by the hybrid plant, there is not a lot of potential to displace the conventional fuel resources currently used in caprolactam production. However, escalating energy prices and new demands for caprolactam could change this conclusion. For example, Monsanto Chemicals has just recently developed a new use for caprolactam (Mathur 1985b).

Table 3-9. Comparison of Caprolactam Production Cost in PNC Process (Electricity Only) and Hybrid Plant (1984 dollars)

Parameters	PNC Process	Hybrid Plant
Photon cost (photons/$ x 10^{24})	21.0	41.6
Production cost ($/metric ton, excluding raw materials cost)	250	126
Plant capacity (metric tons/yr)	60,000[a]	381,000
Current selling price ($/metric ton)	1874[b]	
1983 U.S. production (metric tons)	444,000[c]	

[a] European Chemical News (1976).
[b] Chemical Marketing Reporter (1984).
[c] Chemical and Engineering News (1984).

SECTION 4.0

CONCLUSIONS AND RECOMMENDATIONS

4.1 CONCLUSIONS

The equipment and economic trade-offs of a hydrogen-producing hybrid plant versus the thermal-only plant are as follows:

- If a portion of the solar spectrum can be more efficiently utilized by the quantum process rather than the thermal process, then the heliostat field required may be reduced in size.
- The thermal portion of the hybrid plant may also be reduced in size in proportion to the fraction of energy diverted to the quantum process.
- Additional costs arise from adding the quantum receiver and cooler.

This study has identified the following areas in which research is needed to make a hydrogen-producing hybrid plant attractive:

- Conventional electrolysis techniques must achieve the goal of 85% stack efficiency.
- Problems associated with the photoelectrochemical decomposition of water (low efficiencies, photocorrosion, and material problems) need to be resolved.
- The beam-splitting and reflection performance of the holograms needs to be improved.

Assuming optimistic cost and performance goals, our analysis showed that a small reduction (10%) in hydrogen production cost is possible, compared with the base-case thermal plant. When more realistic goals are assumed, the hybrid plant shows no cost advantage. Thus, there is little economic incentive to pursue the development of a hydrogen-producing hybrid plant.

The analysis of caprolactam production cost shows that a hybrid plant could produce caprolactam cheaper today than the PNC methods do. A 100-MW_e hybrid plant would supply nearly the entire 1984 U.S. output; thus, there would be no large displacement of conventional fuel resources. This is only a tentative conclusion, however, since a more comprehensive analysis of engineering requirements, thermal process requirements, and a high-flux photochemical receiver must be done. But an important point concerning hybrid conversion is illustrated; that is, economic attractiveness depends on the product. For caprolactam production, substituting solar photons for high-valued electricity results in lower production cost. However, before a thermally decoupled hybrid system can work, an efficient method of beam splitting must be found. Achieving high efficiency may be possible with holograms, but further development work is needed.

4.2 RECOMMENDATIONS

Results have shown that significant improvements in photoelectrochemical water decomposition and electrolyzer technology are needed to make hydrogen production by a hybrid plant attractive. Since only a small cost advantage relative to a thermal-only plant could be realized, assuming a photoelectrochemical process operating at theoretical efficiency, hydrogen production by a hybrid plant should not be given any further consideration. However, the feasibility of hybrid-plant production of high-value chemicals should be investigated, particularly in regard to caprolactam. A preliminary program investigating the use of sunlight for caprolactam production should be initiated. Information on the engineering and photochemical aspects of caprolactam production should be gathered so that a detailed systems study can be performed.

It is clear from this discussion that some hybrid systems do show considerable potential. However, specific factors such as the quantum process to be used, the performance of the beam splitter, and the thermal process to be used must determine whether a particular hybrid system is attractive. Many thermally decoupled and thermally coupled systems have not been addressed in this study. For instance, a hybrid system that generates electricity using photovoltaics and a thermal conversion process could be conceived. Even multiple quantum systems of different band gaps in combination with thermal technology are a possibility. Systems combining the technologies of thermal, electric, and chemical conversion are also possible. Some of these schemes should be analyzed so that a clearer understanding of the possibilities for hybrid conversion are known.

In this study, holograms are used for the beam splitter because they have the greatest potential to achieve high efficiency at low cost. At present, holograms operate in narrow-wavelength regions at low efficiencies. But because of their potential as cheap solar energy beam splitters and concentrators for hybrid and conventional solar energy systems, research and development work on holograms should continue. We suggest that a conference be held on holographic technology involving industry, academic, and national laboratory participation. The focus of such a meeting should be to define the limits of holographic technology. From this, the need for and value of further work in the area should be defined.

SECTION 5.0

REFERENCES

Apley, W. J., et al., 1980, Assessment of Generic Solar Thermal Systems for Large Power Applications: Vol. I, Analysis of Electric Power Generating Costs for Systems Larger than 10 MW_e, PNL-3533, Richland, WA: Pacific Northwest Laboratory.

Batchelder, J. S., A. H. Zewail, and T. Cole, 1979, "Luminescent Solar Concentrators, 1: Theory of Operation and Techniques for Performance Evaluation," Applied Optics, Vol. 18, No. 18, pp. 3090-3110.

Batchelder, J. S., A. H. Zewail, and T. Cole, 1981, "Luminescent Solar Concentrators, 2: Experimental and Theoretical Analysis of Their Possible Efficiencies," Applied Optics, Vol. 20, No. 21, pp. 3733-3754.

Beller, M., and A. Mezzina, 1983, Chemical/Hydrogen Energy Systems Multi-Year R&D Plan, BNL-51686, Uptown, Long Island, NY: Brookhaven National Laboratory.

Biddle, J., and D. Peterson, 1983, Solar Photochemical Process Engineering for Production of Fuels and Chemicals, DOE/JPL-1060 (Draft), Pasadena, CA: Jet Propulsion Laboratory.

Bilgen, E., and C. Bilgen, 1982, "Hydrogen as a Vector for Central Receiver Solar Utilities," International Journal of Hydrogen Energy, Vol. 7, No. 12, pp. 977-984.

Bilgen, C., and E. Bilgen, 1984, "An Assessment on Hydrogen Production Using Central Receiver Solar Systems," International Journal of Hydrogen Energy, Vol. 9, No. 3, pp. 197-204.

Bloss, W. H., M. Griesinger, and E. R. Reinhardt, 1982, "Dispersive Concentrating Systems Based on Transmission Phase Holograms for Solar Applications," Applied Optics, Vol. 21, No. 20, pp. 3739-3742.

Bolton, J. R., A. F. Haught, and R. T. Ross, 1981, "Photochemical Energy Storage: An Analysis of Limits," in Photochemical Conversion and Storage of Solar Energy, edited by J. S. Connolly, New York, NY: Academic Press, pp. 297-339.

Bonner, M., T. Botts, J. McBreen, A. Mezzina, F. Salzano, and C. Yang, 1982, "Status of Advanced Electrolytic Hydrogen Production in the United States and Abroad," in Hydrogen Energy Progress-IV, Proceedings of the 4th World Hydrogen Energy Conference, International Association for Hydrogen Energy, pp. 117-127.

Chemical and Engineering News, June 11, 1984, "Facts & Figures," p. 37.

Chemical Marketing Reporter, October 8, 1984, p. 35.

Corion Corporation, 1983, Optical Filters and Coatings, Holliston, MA, p. 46.

European Chemical News, February 27, 1976, "Toray Claims Energy Savings in Caprolactam Production," p. 25.

Fickett, A. P., and F. R. Kalhammer, 1977, "Water Electrolysis," in Hydrogen: Its Technology and Implications, Vol. 1, edited by K. E. Cox and K. D. Williamson, Cleveland, OH: CRC Press.

Fischer, M., 1978, "Industrial Applications of Photochemical Syntheses," Agnew. Chem. Int. Ed. Engl., Vol. 17, pp. 16-26.

Friedman, P. S., 1980, "Progress on the Development of Luminescent Solar Concentrators," in SPIE 24th International Technical Symposium, San Diego, CA, July 28-August 1, 1980.

Goetzberger, A., and V. Witter, 1981, "Fluorescent Planar Collector-Concentrators: A Review," Solar Cells, Vol. 4, pp. 3-23.

Gratzel, M., 1981, "Photoinduced Water Splitting in Heterogeneous Solution," in Photochemical Conversion and Storage of Solar Energy, edited by J. S. Connolly, New York, NY: Academic Press, pp. 131-160.

Hammerli, M., 1984, "When Will Electrolytic Hydrogen Become Competitive?" International Journal of Hydrogen Energy, Vol. 9, No. 112, pp. 25-51.

Haught, A. F., February 1984, "Physics Considerations of Solar Energy Conversion," Journal of Solar Energy Engineering, Vol. 106, pp. 3-15.

Herman, A. M., 1982, "Luminescent Solar Concentrators--A Review," Solar Energy, Vol. 29, No. 4, pp. 323-329.

Hulme, P., and P. E. Turner, November 1967, "Photochemical Route to Caprolactam," Chemical and Process Engineering, pp. 96-100.

Ito, Y., and S. Matsuda, 1969, "Photochemical Synthesis of Epsilon-Caprolactam," Annals of the New York Academy of Science, Vol. 147, No. 16, pp. 618-624.

Jannson, T., 26 April 1984, personal communication, National Technical Systems, Los Angeles, CA.

Johnson, D. H., 1983, "Quantum and Thermal Conversion of Solar Energy to Useful Work," SERI/TP-252-2137, presented at Solar Thermal Workshop, Atlanta, GA, 7-8 Sept. 1983.

Johnson, D., and M. Karpuk, editors, 1983, Proceedings of the Solar Thermal/Photochemical Conversion Workshop, SERI/CP-252-2026, Golden, CO: Solar Energy Research Institute.

Laity, N. W., et al., 1980, Assessment of Solar Thermal Options for Small Power Systems, Vols. 1, 2, 3, PNL-4000, Richland, WA: Pacific Northwest Laboratory.

Ludman, J. E., 1982, "Holographic Solar Concentrator," Applied Optics, Vol. 21, No. 17, pp. 3057-3058.

Mathur, V. K., 1985a, Solar Photochemical Production of Fuels and Chemicals: Technical Report, Task III(a), SERI/SRR-253-2837, Golden, CO: Solar Energy Research Institute.

Mathur, V. K., 1985b, University of New Hampshire, Durham, NH, personal communication.

Matson, R., R. Bird, and K. Emery, 1981, Terrestrial Solar Spectra, Solar Simulation, and Solar Cell Efficiency Measurement, SERI/TR-612-964, Golden, CO: Solar Energy Research Institute.

National Technical Systems, 1983, Spectrum-Splitting Holoconcentrators: Annual Report to the Department of Energy, DE-AC03-81ER10836, Los Angeles, CA.

Nozik, A. J., 1981, "Photoelectrosynthesis at Semiconductor Electrodes," in Photochemical Conversion and Storage of Solar Energy, edited by J. S. Connolly, New York, NY: Academic Press, pp. 271-295.

Nutall, L. J., and J. H. Russell, 1979, "Solid Polymer Electrolyte Water Electroysis Development Studies," Proceedings of the 2nd World Hydrogen Energy Conference, Vol. 1, International Association for Hydrogen Energy, pp. 391-402.

Offenhartz, P. O'D., R. H. Micheels, and A. D. Darrow, 1982, Use of Inorganic Materials for Phosphorescent Concentrating Solar Cells, Draft Final Report to Photovoltaics Program Office, Golden, CO: Solar Energy Research Institute.

Optical Society of America, 1978, Handbook of Optics, New York, NY: McGraw-Hill, pp. 15-28.

Parkinson, B., 15 August 1984, personal communication, Solar Energy Research Institute, Golden, CO.

Peters, M. S., and K. D. Timmerhaus, 1980, Plant Design and Economics for Chemical Engineers, 3rd ed., New York, NY: McGraw-Hill.

Ross, R. T., 1967, "Some Thermodynamics of Photochemical Systems," Journal of Chemical Physics, Vol. 46, No. 12, pp. 4590-4593.

Ross, R. T., and T. Hsiao, 1977, "Limits on the Yield of Photochemical Solar Energy Conversion," Journal of Applied Physics, Vol. 48, No. 11, pp. 4783-4785.

Russell, J. H., 1981, "An Update of Solid Polymer Electrolyte Water Electrolysis Programs at General Electric," in Proceedings of the 3rd World Hydrogen Energy Conference, Vol. 1, International Association for Hydrogen Energy, pp. 3-13.

Sansregret, J., J. M. Drake, W. R. L. Thomas, and M. L. Lesiecki, 1983, "Light Transport in Planar Luminescent Solar Concentrators: The Role of DCM Self-Absorption," Applied Optics, Vol. 22, No. 4, pp. 573-577.

Shockley, W., and H. J. Queisser, 1961, "Detailed Balance Limit of Efficiency of p-n Junction Solar Cells," Journal of Applied Physics, Vol. 32, pp. 510-519.

Taverna, M., and M. Chiti, November 1970, "Compare Routes to Caprolactam," Hydrocarbon Processing, pp. 137-145.

Thomas, W. R. L., J. M. Drake, and M. L. Lesiecki, 1983, "Light Transport in Planar Luminescent Solar Concentrators: The Role of Matrix Losses," Applied Optics, Vol. 22, No. 21, pp. 3440-3450.

Wolfson, R. G., 1983, "Large-Scale Production Potential of GaAs/Si for High Efficiency Flat-Plate Modules," in Photovoltaics Advanced Research and Development 5th Annual Review Meeting, SERI/CP-311-2011, Golden, CO: Solar Energy Research Institute.

APPENDIX A

DICHROIC MIRROR HELIOSTAT ANALYSIS

This work has focused on extending the treatment of beam-splitting efficiency for the dichroic mirror heliostat. We examine the effect of the second pass through the dichroic mirror by the transmitted portion of the solar spectrum and differences between long- and short-wavelength transmitting mirrors. Finally, a simple analysis of solar tracking by the two-mirror heliostat is presented.

A.1 EFFICIENCY

The fraction of solar radiation reflected to each receiver on the tower will be affected by the dichroic mirror type, e.g., a short- or long-wavelength transmitting mirror. The choice needs to be analyzed carefully, since there are differences in transmission characteristics for the two cases. In the two-mirror heliostat configuration, an analysis is also needed of total system efficiencies, since additional optical losses of the transmitted light occur as a result of reflection from the back-mirrored surface and as a result of the second pass through the dichroic mirror. The analysis in Section 2.0 has been extended to the case for the long-wavelength transmitting mirror and dichroic mirror in the heliostat configuration.

Since a cutoff wavelength of 620 nm was previously chosen for the quantum process, this is the cutoff wavelength at which the analysis is done. The losses for the long-wavelength transmitting mirror were calculated in much the same way as those for a short-wavelength transmitting mirror. Below the 620-nm cutoff wavelength, 85% of the incident light was assumed to be reflected to the quantum receiver, and the remainder lost. At above the cutoff wavelength, data from Corion (1983) were used: 80% transmission from the cutoff wavelength to 2200 nm, and the rest assumed lost. From 2200 nm to higher wavelengths, another 40% is assumed to be transmitted and the rest, lost.

To calculate the energy available from the dichroic mirror heliostat, the back reflective surface was assumed to be an excellent mirrored surface having a 95% reflectivity. The amount of energy lost traversing back through the dichroic mirror is the same as previously determined: 65% for the short-wavelength transmitting mirror and 80% for the long-wavelength transmitting mirror. The results of the calculations are shown in Table A-1 for a 620-nm cutoff wavelength and dichroic mirrors either alone or in the heliostat configuration.

A comparison of the results for the dichroic mirror alone shows that the energy available to the quantum or thermal process depends heavily on which type of mirror is used. More energy is available to the process that collects the reflected radiation. The same trend is also evident in the heliostat results. A severe loss is incurred on the portion of the spectrum transmitted and reflected back through the dichroic mirror. The largest losses occur for the long-wavelength transmitting mirror, because 67% of the available energy

Table A-1. Beam-Splitting Efficiencies for a 620-nm Cutoff Wavelength and Short- and Long-Wavelength Transmitting Dichroic Mirrors Alone or in the Heliostat Configuration

Configuration[a]		Fraction of Energy Available to Process or Lost		
		Quantum Process (%)	Thermal Process (%)	Lost (%)
SWT	Alone	19.6	60.0	20.4
	Heliostat	12.1	60.0	27.9
LWT	Alone	27.1	55.8	17.1
	Heliostat	27.1	42.4	30.5

[a]SWT = short-wavelength transmitting dichroic mirror.
LWT = long-wavelength transmitting dichroic mirror.

must be transmitted through the dichroic mirror twice, whereas in the short-wavelength transmitting configuration, the fraction is only 33%.

A.2 TRACKING

The simplest method of obtaining a second focus point on a tower with a dichroic mirror is to tilt the surface with respect to the back mirror while keeping the upper and lower edges of the dichroic mirror parallel to the back mirror. The question that arises is whether the focus point will be maintained at the same spot on the tower, assuming that the back mirror is controlled by the normal heliostat steering equations. If not, some type of drive mechanism may be necessary to position the dichroic mirror to maintain the focus point at the same spot.

From the geometry of the mirrors, the dichroic mirror will track the sun in the azimuthal direction in the same way as the bottom mirror, since the horizontal components of the normal vectors to the mirrored surfaces are parallel. Thus, the focus point will be maintained on the tower, but at a different vertical elevation. The vertical variation of the focus point as a function of the sun's altitude remains to be determined.

The situation is illustrated in Figure A-1, where

ϕ = sun's altitude

θ = angle between dichroic and back mirror

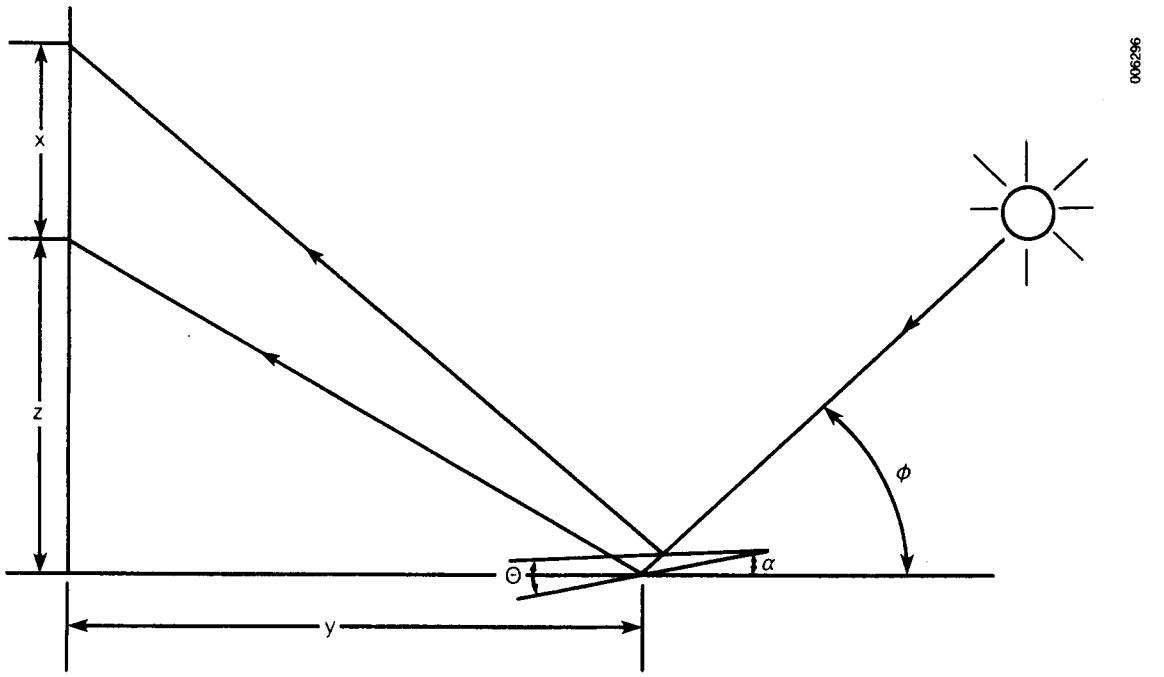

Figure A-1. Path and Geometry of Solar Beam Reflected by a Dichroic Mirror Heliostat

α = angle between back mirror and horizon

y = distance from tower to heliostat (m)

z = distance from ground to first receiver (m)

x = distance between first and second receiver (m).

The reason that the beam varies in the vertical direction is that the light beam, as shown in Figure A-2, strikes the dichroic mirror at different locations on the mirror, depending on the sun's altitude, and thus at different mirror separation distances. This results in another beam variation in addition to the normal cosine variation. The vertical variation would be acceptable if it were small enough, or compensated by adding an additional drive mechanism to change the angle between the mirrors.

To determine the magnitude of the beam variation, a simple two-dimensional analysis was performed. Using Figures A-1 and A-2 (the latter showing more details of the mirror geometry needed for the derivation), a relationship between ϕ and x can be derived. From a simple addition of angles,

$$\gamma = \phi - \alpha \ , \qquad \text{(A-1)}$$

and since the angle of incidence equals the angle of reflection,

$$\beta = \gamma - \alpha \ ,$$

or

$$\beta = \phi - 2\alpha \ , \qquad \text{(A-2)}$$

from Eq. A-1.

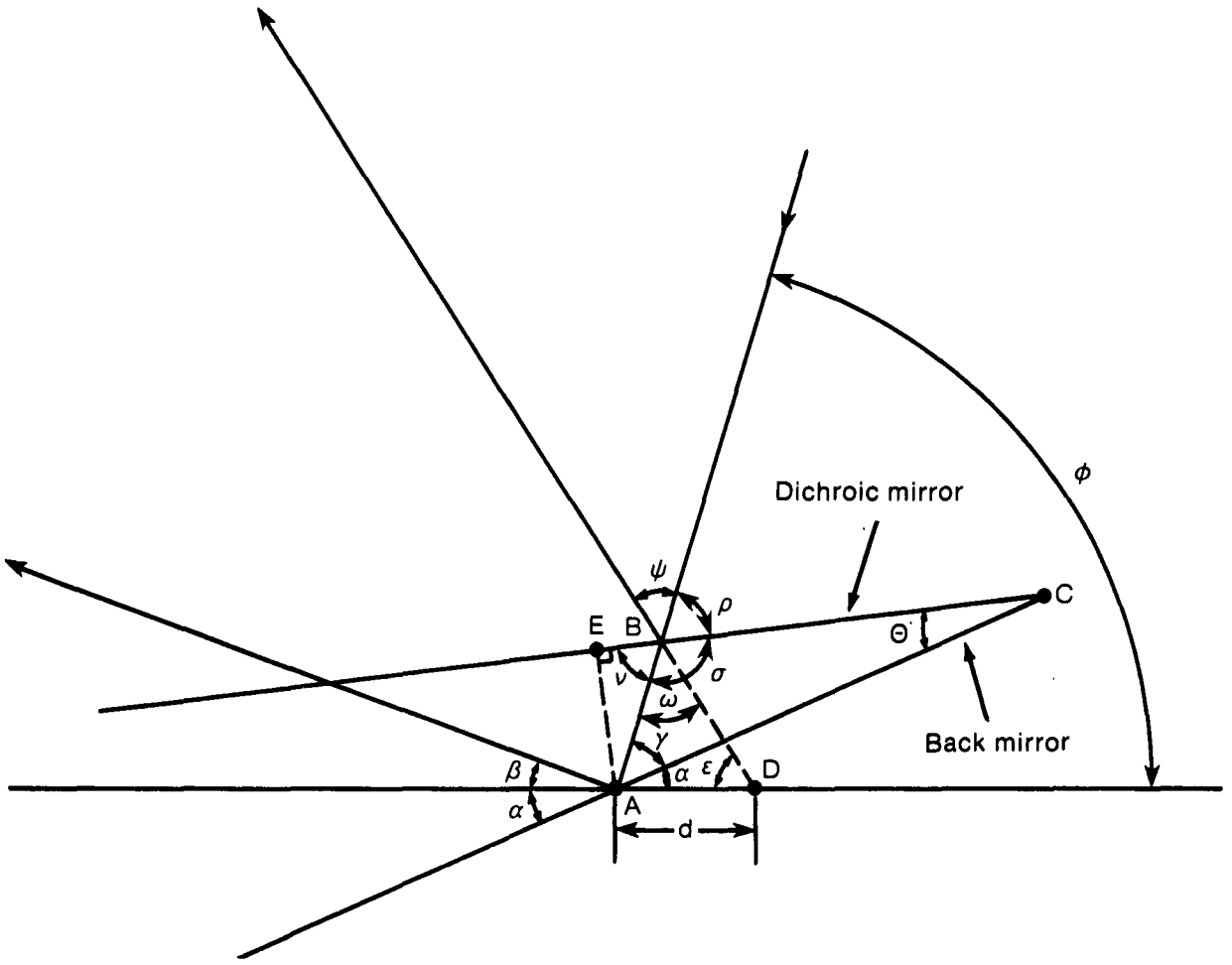

Figure A-2. Geometry Needed to Analyze the Dichroic Mirror Heliostat Concept

Adding angles in triangle ABC:

$$\sigma = \pi - \theta - \gamma \ ,$$

or

$$\sigma = \pi - \theta + \alpha - \phi \ , \qquad \text{(A-3)}$$

again using Eq. A-1. From supplementary angles,

$$\rho = \pi - \sigma \ ,$$

or

$$\rho = \theta + \phi - \alpha \qquad \text{(A-4)}$$

using Eq. A-3.

Again, using the law of reflection and supplementary angles,

$$\Psi = \pi - 2\rho \ ,$$

or

$$\Psi = \pi - 2(\theta + \phi - \alpha) \ , \qquad \text{(A-5)}$$

using Eq. A-4. One last relationship needed between the angles can be determined by looking at triangle ABD and summing angles, first noting that $\omega = \Psi$; then,

$$\varepsilon = \pi - \Psi - \phi \ ,$$

or

$$\varepsilon = \phi - 2\alpha + 2\theta \ , \qquad \text{(A-6)}$$

using Eq. A-5.

From the appropriate angles, the length of element d can be calculated. First, notice from triangle AEC that

$$\sin\theta = \frac{AE}{AC} \ , \qquad \text{(A-7)}$$

where AE and AC are the distances between the two respective points. From triangle AEB and since $\nu = \rho$:

$$\sin\nu = \sin\rho = \frac{AE}{AB} \ ,$$

or, rearranging:

$$AB = \frac{AE}{\sin\rho} = \frac{AE}{\sin(\theta + \phi - \alpha)} \ , \qquad \text{(A-8)}$$

from Eq. A-4. Combining Eqs. A-7 and A-8 and defining AC = a, the distance AB is

$$AB = \frac{a \sin\theta}{\sin(\theta + \phi - \alpha)} \ . \qquad \text{(A-9)}$$

Now, using the Law of Sines on triangle ABD gives

$$\frac{d}{\sin\Psi} = \frac{AB}{\sin\varepsilon} \ ,$$

and then, using Eqs. A-5, A-6, and A-9 yields

$$d = \frac{c \sin\theta \sin(\pi - 2\theta - 2\phi + 2\alpha)}{\sin(\theta + \phi - \alpha)\sin(\phi - 2\alpha + 2\theta)} \ . \qquad \text{(A-10)}$$

The next task is to derive the relation between x and ϕ. From Figures A-1 and A-2, we find

$$\tan\beta = z/y \ ,$$

or, using Eq. A-2 and rearranging:

$$\phi - 2\alpha = \arctan (z/y) . \qquad \text{(A-11)}$$

At a given distance from the tower y, $\phi - 2\alpha$ is a constant, since z is also constant; thus, ϕ and α cannot be independent. Also, from the figures,

$$\tan \varepsilon = \frac{x + z}{y + d} ,$$

and using Eq. A-6 and solving for x gives

$$x = (y + d) \tan (\phi - 2\alpha + 2\theta) - z. \qquad \text{(A-12)}$$

If $d = 0$, then $\theta = 0^{\circ}$, i.e., the mirrors are flat together, and $x = 0$ from the substitution of Eqs. A-11 into A-12, and Eq. A-12 holds in the limiting case.

Using Eq. A-12, the height of the second focus point x can be examined as a function of the angle θ between the mirrors, the sun's altitude ϕ, and the distance y from the tower. Since the intent is to eliminate a drive motor that would position the mirrors with respect to each other, Eq. A-12 was analyzed by finding the optimum θ for a given distance y which produced the least variation from a chosen x. The values assumed for x, z, and a, the latter the mirror half-length, were then varied to determine their effects on beam variation.

The results have been plotted in Figure A-3. Curve 1 shows the maximum variation from the assumed focus spot for $z = 70$ m, $x = 20$ m, and $a = 1$ m as a function of distance from the tower. The angle between the mirrors θ needed to obtain the results of Curve 1 are shown by Curve 5. At increasing distance from the tower the beam variation decreases, but the angle between the mirrors also decreases to values that may be difficult to obtain precisely. Curve 4 shows the effect of being 0.1° off the optimum angle. Now, beam variation increases with distance from the tower and quickly approaches unacceptable values. Curve 2 shows beam variation for $z = 50$ m, $x = 40$ m, and $a = 1$ m, and this suggests that it is better to place the receivers closer together. But as the receivers are moved closer together, the angle between the mirrors decreases, so there is a trade-off between how small the angle between the mirrors can be and the acceptable beam variation. Curve 3 shows conditions for $z = 50$ m, $x = 40$ m, and $a = 3$ m, which is the same as Curve 2 except that the mirror half-length has been increased; it shows that increasing mirror length increases beam variation.

The conditions for Curve 2 are the closest to the tower dimensions necessary for the hybrid system. Mirrors on the heliostats usually consist of smaller sections, each well within the 1-m half-length. The maximum beam variation for Curve 2 was 42 cm, which is an acceptable variation. This would eliminate the need for a drive system to position the mirrors if the optimum angle can be maintained. The other option is to allow the variation to take place and oversize the receiver, although concentration would be reduced.

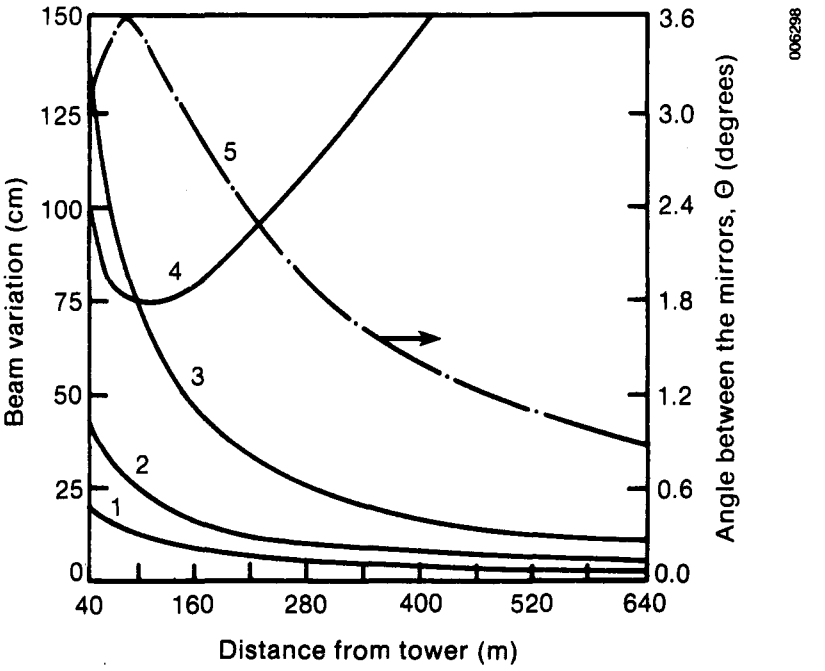

Figure A-3. Variation of Light Beam from Predetermined Focus Point as a Function of Distance from Central Receiver Tower for (1) z = 70 m, x = 20 m, and a = 1 m; (2) z = 50 m, x = 40 m, and a = 1 m; (3) z = 50 m, x = 40 m, and a = 3 m; (4) same conditions as for 1 but with θ varied 0.1° from optimum angle; and (5) θ as a function of distance from tower at conditions as for 1.

APPENDIX B

ESTIMATION OF PHOTOELECTROCHEMICAL RECEIVER COST

Cost of the photoelectrochemical receiver is based only upon the design presented in Figure 3-3. This includes the cost for glass pipe and the anodic and cathodic materials. Factors have been included for structural and installation requirements. All costs have been computed on the basis of 1980 dollars and used optimistic cost goals for electrolyzer and semiconductor technology.

As previously explained, the conceptual configuration of the receiver is of vertical glass pipes ringing the tower. A cross-sectional view of one glass pipe used in cost estimating is shown in Figure B-1. The diameter of glass pipe was arbitrarily chosen as 2.54 cm (1.0 in.). The diameter of the inner cathode was also arbitrarily chosen as 1.90 cm (0.75 in.); this is an important number needed to estimate the area of the semiconductor and conductive substrates required. It was assumed that these materials would cover only half of the cathode surface (i.e., the half exposed to sunlight).

The cost of the photoelectrochemical receiver is shown in Table B-1 and was estimated on the basis of illuminated semiconductor area, since this is the important factor controlling receiver size. The basis column in the table shows the factor required to convert cost based on illuminated semiconductor area on a per square meter basis. This is necessary because the glass pipe cost on a per planar area basis must be corrected for the actual illuminated area inside the tube. The basis for the anode and NaFion® membrane was assumed to be 1.0. Since a specific cost breakdown on these individual materials was not available, it would be senseless to estimate any further. Estimation of cathode cost is even more difficult; however, it is reasonable to assume that a conductive substrate and the rest of the cathode will cost more than the semiconductive layer ($\$22/m^2$), since it is likely that deposition and material cost are nearly the same. But it is not likely to exceed the cost for the anode plus the semiconductive layer ($\$54/m^2 + \$22/m^2 = \$76/m^2$). A value half way between the two was arbitrarily chosen as the cost for the rest of the cathode and the conductive substrate. The installation and investment factors are shown at the bottom of the table in the basis column and are multiplied times the total material cost to determine the total cost for the receiver.

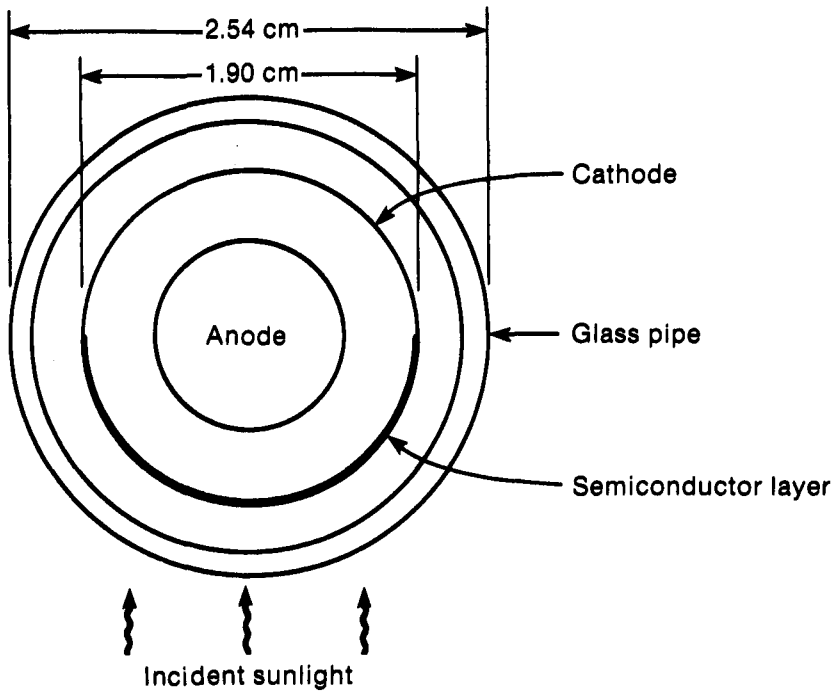

Figure B-1. Cross-Sectional View of One Glass Pipe in the Photoelectrochemical Receiver

Table B-1. Photoelectrochemical Receiver Cost Estimation (1980 dollars)

Item	Cost ($/m^2)	Basis	Adjusted Cost ($/m^2)	Source
Glass pipes	600	0.85	510	Peters and Timmerhaus (1980)
Semiconductor	22	1.0	22	Wolfson (1983)
Cathode plus conductive substrate	49	1.0	49	Assumed
Anode plus NaFion®	54	1.0	54	Nutall and Russell (1979)
Total material cost			662	
x installation factor		1.8	1,192	
x investment factor		1.95	2,324	
Total cost			2,324	

DISTRIBUTION

Allied Chemical Company
P.O. Box 1021R
Morristown, NJ 07960
Mr. Robert Armburst

Battelle Pacific NW Laboratory
P.O. Box 999
Richland, WA 99352
Dr. Ben Johnson

Black and Veatch Consulting Engineers
1500 Meadow Lake Parkway
Kansas City, MO 64114
Dr. Charles Grosskreutz

Bowman, Dr. Melvin
Consultant
360 Andanada
Los Alamos, NM 87544

Department of Energy/HQ
1000 Independence Ave., SW
Washington, DC 20585
Dr. H. Coleman
Mr. Frank Wilkins

England, Dr. Christopher
Consultant
Engineering Research Group
138 West Pomona Ave.
Morrovia, CA 91016

Gas Research Institute
8600 West Bryn Mawr Ave.
Chicago, IL 60631
Mr. Keith Davidson

Georgia Institute of Technology
Atlanta, GA 30332
Mr. Robert Cassanova

Lawrence Berkeley Laboratory
Building 90-2024
University of California
1 Cyclotron Road
Berkeley, CA 94720
Dr. Arlan Hunt

Sandia National Laboratories
Solar Department 8453
Livermore, CA 94550
Mr. J. D. Swearengen

University of Hawaii at Manoa
Hawaii Natural Energy Institute
Homes Hall Room 246
2540 Dole Street
Honolulu, HI 96822
Dr. Mike Antal

University of Houston
4800 Calhoun
106 SPA Building
Houston, TX 77004
Dr. Alvin Hildebrandt

University of Minnesota
Dept. of Mechanical Engineering
Minneapolis, MN 55455
Dr. Edward Fletcher

University of New Hampshire and
College of Engineering and Physical Sciences
Kingsbury Hall - 260
Durham, NH 03824
Dr. V. K. Mathur

Document Control Page	1. SERI Report No. SERI/TR-232-2565	2. NTIS Accession No.	3. Recipient's Accession No.

4. Title and Subtitle
Engineering Systems Analysis of a Hybrid Quantum/Thermal Process for Fuels and Chemicals Production

5. Publication Date
November 1985

6.

7. Author(s)
D. Schell, M. Karpuk, R. West

8. Performing Organization Rept. No.

9. Performing Organization Name and Address
Solar Energy Research Institute
1617 Cole Boulevard
Golden, Colorado 80401

10. Project/Task/Work Unit No.
5103.23

11. Contract (C) or Grant (G) No.
(C)
(G)

12. Sponsoring Organization Name and Address

13. Type of Report & Period Covered
Technical Report

14.

15. Supplementary Notes

16. Abstract (Limit: 200 words)
A systems analysis of a thermally decoupled quantum/thermal solar conversion system is performed to determine the relative cost advantage of this system over a thermal-only system. This hybrid system splits the solar spectrum into two parts; sending the short-wavelength fraction to a quantum receiver and the long-wavelength fraction to a thermal receiver. An efficiency greater than either system acting alone can be achieved. The primary analysis is done on a 100 MWe central power tower using a Rankine cycle power plant to convert thermal energy to electrical energy and that then produces hydrogen by electrolysis. The hybrid plant uses the same thermal conversion system, and adds a photoelectrochemical process for the quantum system. When optimistic assumptions regarding the performance of the photoelectrochemical process are made, a 10% reduction in hydrogen production cost is achieved when compared to the thermal-only system. There is little or no advantage to the hybrid system when the assumptions are less optimistic. A brief, but similar analysis of a hybrid system for the production of a high value chemical, caprolactam, shows that a significant cost reduction is possible. These results suggest that the economic attractiveness of hybrid conversion depends on the product.

17. Document Analysis
a. Descriptors
Absorption; Beam Splitting; Dichroism; Efficiency; Holography; Hydrogen Production; Luminescent Concentrators; Mirrors; Solar Concentrators; Solar Radiation; Spectra; Wavelengths

b. Identifiers/Open-Ended Terms

c. UC Categories
62c

18. Availability Statement
National Technical Information Service
U.S. Department of Commerce
5285 Port Royal Road
Springfield, Virginia 22161

19. No. of Pages
68

20. Price
A04

Form No. 0069 (3-25-82)